RESONANT FREQUENCIES IN WEB LINES AND FILTERING OF WEB TENSION

By

YU DIAO

Bachelor of Engineering
Shanghai Jiao Tong University
Shanghai, China
2003

Submitted to the Faculty of the
Graduate College of the
Oklahoma State University
in partial fulfillment of
the requirements for
the Degree of
MASTER OF SCIENCE
December, 2008

RESONANT FREQUENCIES IN WEB LINES AND FILTERING OF WEB TENSION

Thesis Approved:

Thesis Adviser, Dr. Prabhakar R. Pagilla

Committee Member, Dr. John J. Shelton

Committee Member, Dr. Gary E. Young

Dean of the Graduate College

ACKNOWLEDGMENTS

I would first like to express my sincerest appreciation to my advisor, and thesis committee chairman, Dr. Prabhakar R. Pagilla for his intelligent supervision, constructive guidance, inspiration, and friendship. He motivated me to work on the web longitudinal behavior and tension sensing project from the very beginning. Without his guidance and expertise in supervising the research, I would not have completed this work. I have been learning from his research experience, his kindness and his enthusiasm. I believe I will benefit from the experience all through the rest of my life.

I would like to extend my warmest thanks to my other doctoral committee members: Dr. John J. Shelton, and Dr. Gary E. Young for their support and suggestions in completion of this research. Their guidance and understanding made the development of this thesis a positive learning experience.

I consider myself very fortunate for being able to work under their supervision. I shall be forever thankful to them for providing this glorious opportunity to learn.

I would like to thank my colleagues at Oklahoma State University, Yunfei Zou, Aravind Seshadri, Carlo Branca, Mauro Cimino, Tan Chai and Pramod Raul for their help and discussion all through the time of the work. They are among the finest people I know and are a joy to work with.

Finally, but not least, I would like to express my appreciation to my parents, Xuefeng Diao and Youjun Ge, for their edify, love and support all though my life, especially for giving me the encouragement to pursue the advanced academic degree.

TABLE OF CONTENTS

LIST OF TABLES

Table Page

LIST OF FIGURES

Figure Page

NOMENCLATURE

A	:	Area of cross-section
$\mathbf{A}_n$	:	$(2n+1) \times (2n+1)$ tridiagonal system matrix
$\mathbf{A}_n^F$	:	$(2n+1) \times (2n+1)$ system matrix based on full linearized tension dynamics
D	:	Matrix determinant
E	:	Modulus of elasticity of web material
EWL	:	Euclid Web Line
J	:	Roller inertia
L	:	Web span length
M	:	Amplitude of the disturbance
N	:	Feedback loop noise
PLC	:	Programmable Logic Controller
P^-	:	Priori estimate
R	:	Roller radius
t	:	Web tension
T	:	Web tension variation
$\hat{T}$	:	Web tension variation estimation
T_s	:	Sampling time
v	:	Web velocity
V	:	Web velocity variation
c	:	Coefficients of the characteristic polynomial of $\mathbf{A}_n$

p	:	Scaled differential operator, s/ν
f	:	Resonant frequency (Hz)
f_1	:	Minimum resonant frequency (Hz)
$\hat{f}_1$	:	Estimate of minimum resonant frequency (Hz)
k	:	Equivalent stiffness, $k = EA/L$
m	:	Equivalent mass, $m = J/R^2$
ρ	:	Web density
s	:	Laplace variable
$\mathbf{x}$	:	State vector
ν	:	Frequency (Hz)
ω	:	Angular velocity (rad/sec)

Subscripts:

i	:	Roller or span index, $i = 0, 1, 2, \ldots$
min	:	Minimum value
n	:	Number of idle rollers, $n = 1, 2, \ldots$
p	:	Related to pull roll
r	:	Reference value
w	:	Related to winder or rewind

CHAPTER 1

INTRODUCTION

Any continuous material whose width is significantly less than its length and whose thickness is significantly less than its width can be described as a web. Examples include paper, plastics, textiles, strip metals, and composites. Web handling refers to the physical mechanics related to the transport and control of web materials through processing machinery. Web processing can be found in many industries today, and it makes it possible to mass produce a rich variety of products from a continuous strip of material. Web tension and velocity are two key variables that influence the quality of the finished web and hence the products manufactured from it.

Through the adoption of high-performance AC motor drives, velocity sensors and advanced control algorithms, web velocity can be controlled reasonably well during both transient and steady state conditions to meet the requirements of industrial production. On the other hand, even though a lot of research work has been done and various control algorithms and solutions have been proposed on web tension control during the past thirty years, the tension control quality still cannot fully satisfy the contemporary high-speed, economical industrial mass production. This is mainly due to the complexity of the nonlinear tension dynamics as well as the fact that the web tension is sensitive to various disturbances such as uneven rollers, driven roller velocity variations and due to signal noises in the sensing feedback loops.

Tension control plays a key role in the quality of the finished web. It is essential to maintain web tension within a specified tolerance range during the entire process operation, which includes startup, steady running, splicing and stop phases of the

web line. For example, if web tension changes during a printing process, the print gets skewed and the web material is wasted. Further, excessive tension variations may cause wrinkles or even tear the web, which increases downtime and material waste and reduces productivity. Thus modeling, verification and control of longitudinal dynamic behavior of web are well worth being studied in the web handling research area.

Two aspects should be further studied in order to improve the tension control performance. The first one is to improve the dynamic model of the web handling system. Extensive research has been done on modeling the driven roller and the web tension dynamics between two driven rollers. But ignoring the existence of the idler rollers in the web path usually leads to the deterioration of the tension control quality as well as the system stability. The study in this thesis partially addresses this problem by investigating the frequency response of an idler system. The other aspect that should be emphasized is the negative effects from noise in the feedback path. How to overcome the impact due to noise is especially important to practical industrial applications where signal interferences are quite common. A Kalman filter is a good tool to solve this problem. The design and implementation of a discrete-time Kalman filter for web tension are also conducted in this thesis.

At last, an effective methodology should be developed in order to verify the research results on a practical web process line. Rather than just staying in the software simulation phase, a researcher should extend his view into the actual web handling platform. This means getting familiar with setup and adjustment of the industrial control systems for the research purpose, realizing algorithms in industrial controllers and collecting experimental data using existing equipment. In addition to that, for the engineers in the web handling industry, this method also provides a cost-effective way to conduct scientific research on their web line instead of just adjusting and tuning the machine by "rules of thumb" and experience.

In the following, a brief introduction to each of the aspects considered in this thesis is presented. A detailed introduction and prior work can be found at the beginning of each chapter.

1.1 The Control System of a Web Process Line

For any research achievements such as development of new system models and control algorithms, it is important to verify them in practical applications before any conclusion can be drawn. This is also true for the research efforts in web handling area: getting verified in a real web process line could be the most persuasive way to show the correctness of the research outcomes. There is still a lot of work to be done from the theoretical derivation and software simulation to the experiment design and implementation on the web line.

Compared to the software simulation, the web processing platform has its own physical limitations which will introduce more restrictions on the experiment design. For example, every driven motor has its own rated output torque. If the required torque generated by the control algorithm is larger than the rated value, torque saturation occurs which may cause more nonlinear and unpredictable system behavior and failure of the motor. Thus a thorough understanding of the hardware specifications and structure of the experiment platform's control system is quite important to conduct successful experiments.

In addition to hardware, there are differences between the control software used in the laboratory environment and the industry application. For the academic researcher in systems and control, MATLAB, dSPACE and LabVIEW are the most commonly used software. They are all based on the computer system and provide a relatively straightforward way to implement advanced algorithms for complex multiple-input and multiple-output (MIMO) system. In addition, they employ similar C languages for programming and algorithm implementation. On the other hand, the control

systems used in industrial web process lines are usually based on Programmable Logic Controller (PLC), and employ different timing and I/O data update mechanisms compared to PC based control systems. The programming languages for industrial control systems are also quite different from C language and are designed with an emphasis on controlling a single-input and single-output (SISO) system and realizing classic control methods such as the PID controller and lead-lag compensators.

All of these issues indicate that mastering both the hardware and software of the industrial control systems is a fundamental step for all web handling research and experimental activities. Considerable amount of work has been done in order to set up and adapt the experiment platform's industrial control system to model verification and for algorithm implementation purposes. A summary of this work has been included in this thesis to show the structure, programming methods and implementations of the control system.

1.2 Resonant Frequencies of an Idler System

Web tension modeling and control have been studied extensively. A dynamic model for the behavior of span tension in a web processing line was developed in [1, 2] based on the conservation of mass principle. The derived span tension dynamics formed the basis for almost all the subsequent work on span tension dynamics. In [3], equations describing web handling system which include tension dynamics as well as driven roller dynamics were derived; an example system was considered to compare torque control versus velocity control of a roll for tension regulation. An overview of lateral and longitudinal dynamic behavior and control of moving webs was presented in [4]. An accurate dynamic model of the web handling machines, which considers the effects of roller's radius change and roller shaft friction, was developed and presented in state space form in [5]; a stable decentralized control scheme was also proposed in the same article.

On the other hand, the dynamic behavior of an idler system consisting of idle rollers and web spans between two consecutive driven rollers was seldom studied in the past: most system modeling and control strategy design processes simply ignore these idlers and treat the web as only one web span between two driven rollers. In fact, these extra idlers and web spans increase the whole web line system's degrees of freedom, and introduce additional system resonant frequencies. The natural frequency of a subsystem comprising of an idle roller separating two free spans was studied in [6]. In [7], Shelton formed the model for an idler system based on linearized web tension dynamics and theoretically calculated the minimum resonant frequencies of an idler system containing up to 5 idlers. Resonant frequencies by software simulation and experiment were explored in [8, 9]. Especially in [9], Carlson followed Shelton's system model to conduct a series experiments on a simple experiment platform and showed some preliminary agreement between the theoretical frequency response and experimental data.

A systematic and detailed study on the idler system's resonant frequencies with any number of idlers has been done in this thesis. Based on a new simplified tension model and the web velocity dynamics on the roller, a generalized state space model of an idler system which will facilitate the analysis and simulation is constructed. Experiments were conducted for different web paths and number of idle rollers on a web platform in order to verify the model. The experimental results show that the proposed model is able to predict the observed tension behavior and the minimum resonant frequency reasonably well. Based on this model, analytical and numerical analyses have been done to reveal the relations between system parameters and the resonant frequencies of the idler system. Further, an estimate of the minimum resonant frequency is derived for the special case of a number of idle roller with equal span lengths, such as the idle rollers and web spans in an accumulator.

1.3 The Kalman Filter for Tension Control

In a web processing line, the quality of the web tension measurement is vital to the system's tension and velocity control performance. Thus a proper filter in the tension feedback loop is highly desired in order to overcome the negative impact of signal interferences.

As a stochastic estimator, the Kalman filter has a better noise rejection capability than deterministic observers in the presence of process and measurement noises. Due to its ease of implementation and relatively low computational workload requirement, the Kalman filter has been widely used in autopilot, computer vision and aerospace areas. But, it is not common to see the implementation of the Kalman filter in the web handling industry. In [10] and [11], the Kalman filter is primarily used to estimate the web's modulus of elasticity. Furthermore, the conclusion which Boulter draws in [10] that the tension measurement is required to obtain a converged state estimation is quite important.

The Kalman filter itself has been studied well in the past, and [12] serves well as a tutorial to the theoretical derivation and practical implementation of a Kalman filter. A linear first order SISO web tension model was developed first; based on that, a tension Kalman filter was designed and the low-pass filter property of the Kalman filter was investigated. Experiments were done on a large web platform to demonstrate the filter's effect on the tension feedback signal.

1.4 Contributions

Literature review of the developments in web tension frequency response reveals the fact that resonant frequencies of an idler system is not studied comprehensively. In addition to that, the application of Kalman filters to web processing lines does not seem to have been done in practice. All of these give a strong motivation to conduct

systematic theoretical studies on these two directions and verify the results through experiments on a real web platform. The contributions of the research work involved in this thesis can be summarized as follows.

1. A detailed introduction to the industrial control system of a web handling processing line, Euclid Web Line (EWL) shown in Figure 1.1, is given. This material will greatly shorten the learning process of the whole control system and facilitate further research on EWL.

2. A new, easy to use state space model of an idler system with any number of spans is proposed and verified by extensive experiments. This model is able to successfully predict the minimum resonant frequency of an idler system.

3. The relationship between the idler system's minimum resonant frequency and the system parameters are revealed through analytical and numerical analysis.

4. A linear web tension error dynamics is developed, and a discrete Kalman filter is designed and implemented in the rewind section of the Euclid Web Line.

5. Comparison experiments were designed on the EWL to demonstrate the tension regulation performance improvement due to the Kalman filter.

6. An experiment and data analysis method used to investigate web tension frequency response is developed using only the existing industrial equipment and software. This method does not only serve the research in this thesis, but also has been applied in other related studies on the EWL, such as investigating the web tension dynamic behavior due to uneven winder roll.

1.5 Organization of the Thesis

The rest of the thesis is organized as follows.

- Chapter 2 gives the introduction and tutorial to the industrial control system of the experimental platform.
- In Chapter 3, the resonant frequencies of an idler system in a web line are addressed.
- The application of a discrete Kalman filter for the web tension control is investigated in Chapter 4.
- Summary and future work are given in Chapter 5.

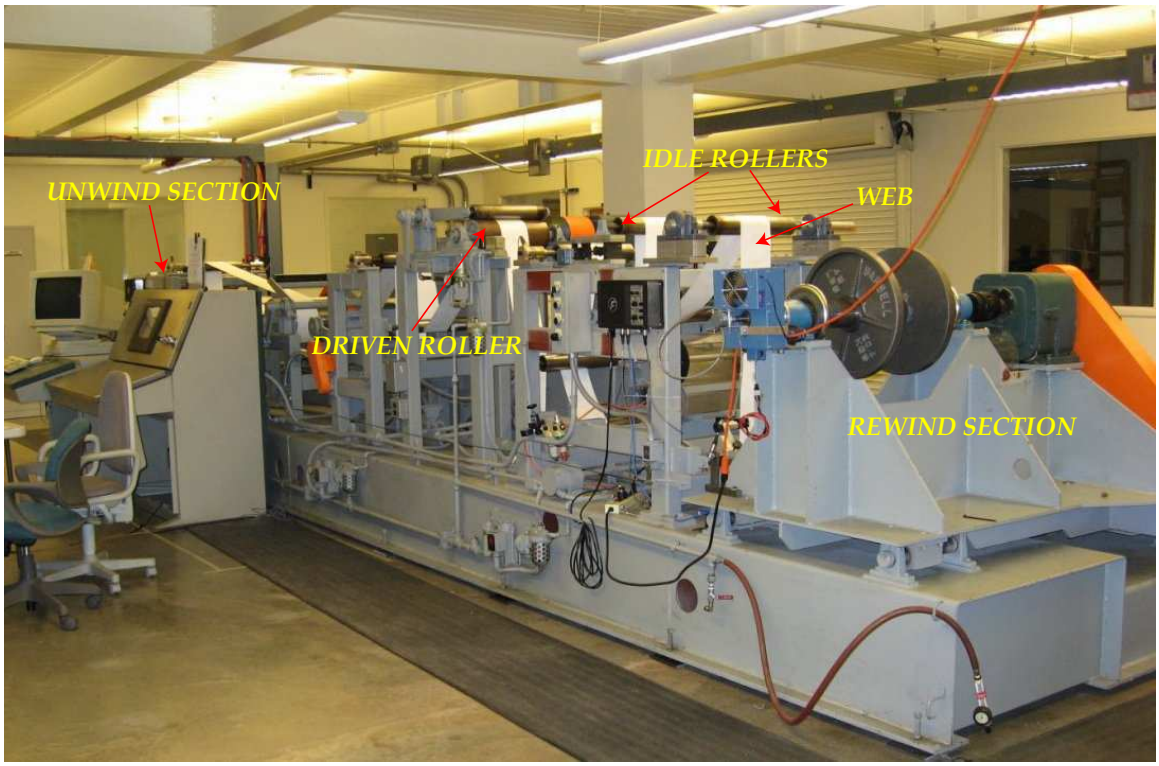

Figure 1.1: Euclid Web Process Line

CHAPTER 2

REAL-TIME IMPLEMENTATION OF WEB LINE CONTROL SYSTEM

Experiments have been conducted in order to verify the system model to predict resonant frequencies and show the effect of the filtering algorithm proposed in this thesis. All experiments were done on an experimental web process line named the Euclid Web Line (EWL) located at the Web Handling Research Center (WHRC), Oklahoma State University. The EWL can mimic most of the features of an industrial web processing line. It is developed with the aim of creating an open-architecture design that allows for modifying the line to conform to research and validation experimentation and provides an ideal platform to implement different control strategies on a practical web processing line.

EWL employs a commercial industrial control system which has been used in many contemporary manufacturing facilities all over the world. The control system adopts a sophisticated and reliable distributed architecture which includes network controllers, AC motors and drives, sensors and field communication network. The hardware of this control system has its own specifications, configuration methods and system architecture. The related software also uses different programming languages and development environment compared with PC based control systems found in most research experiment setups such as MATLAB, dSPACE and LabVIEW. Furthermore, the control system of EWL was originally designed with the goal to control web line's velocity and tension as close as possible to the reference values and reduce the variations and disturbances. On the contrary, in order to facilitate model

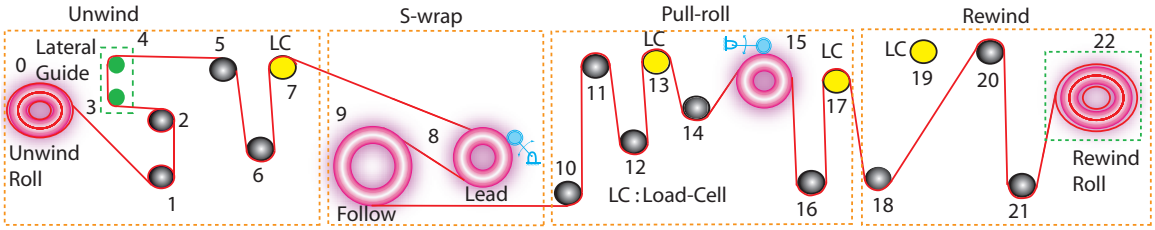

Figure 2.1: Sketch of Euclid Web Line

verification and algorithm demonstration, it is necessary to intentionally inject some disturbances into the web line system during the experiments so that the system behavior at different frequencies can be investigated. Different amplitude and frequency disturbances need to be generated, and a data collection mechanism needs to be developed so that the system responses can be stored for further analysis. Finally, these requirements should be achieved by using the existing equipment to eliminate extra new equipment investment, installation and configuration needs. All of these above indicate that the control system of EWL should be mastered well and adapted accordingly in order to fulfill research and experimental objectives.

In this chapter, the structure of EWL's control system is introduced first. The detailed information about the hardware and software of the control system is revealed. The basic concepts and configuration processes for the controllers, communication bus and AC drives are explained as well, so that the control system can be adapted properly for research purposes. At last, the programming languages of the controller and data collection method are introduced. This chapter is written with the purpose of acting as a tutorial for the beginner to the web process line and an archive of author's understanding and hands-on experience about this industrial control system.

2.1 Introduction to the Euclid Web Line

As the platform for all the experiments conducted in this thesis, the sketch of the EWL is shown in Figure 2.1. The web line can be divided into four sections: the unwind

section, the S-wrap section, the pull roll section, and the rewind section. Normally, one or several sections would function as master speed section which will set the speed of the whole line. In EWL's normal operation status, the S-wrap and pull roll sections function as the master speed which are both running at the line speed given by the operator, whereas the unwind and rewind rollers change their speed around the master speed in order to regulate the web tensions in the unwind and rewind sections. The idler system model validation experiments mentioned in Chapter 3 were done both in pull roll and rewind sections, whereas the implementation of a Kalman filter for web tension control was conducted in the rewind section as detailed in Chapter 4.

Three load cells, installed on rollers 7, 13 and 17, are used to measure the web tensions in different tension zones. Two nip rollers, which are located on rollers 8 and 15, are used to maintain contact of the web with the driven rollers and are loaded by pneumatic actuators. Two controlled lateral guides, located in the unwind and rewind sections, are used to maintain the lateral position of the web on the rollers during web transport. The EWL offers the possibility of modifying the layout of the web line by adding or removing rollers to change the web path. Unless indicated otherwise, the web path used to perform most of the experiments is shown in Figure 2.1.

2.2 Control System Hardware Architecture

The specifications of the hardware have a significant influence on the production capability of the web line, the control strategy selection as well as the final control performance. Figure 2.2 shows the overview of major control system components connected together on the ControlNet communication bus. The hardware of the control system includes five AC motors and drives, five motor velocity feedback encoders, two controllers with I/O modules, three tension load cells, one HMI touchscreen, communication modules and cables.

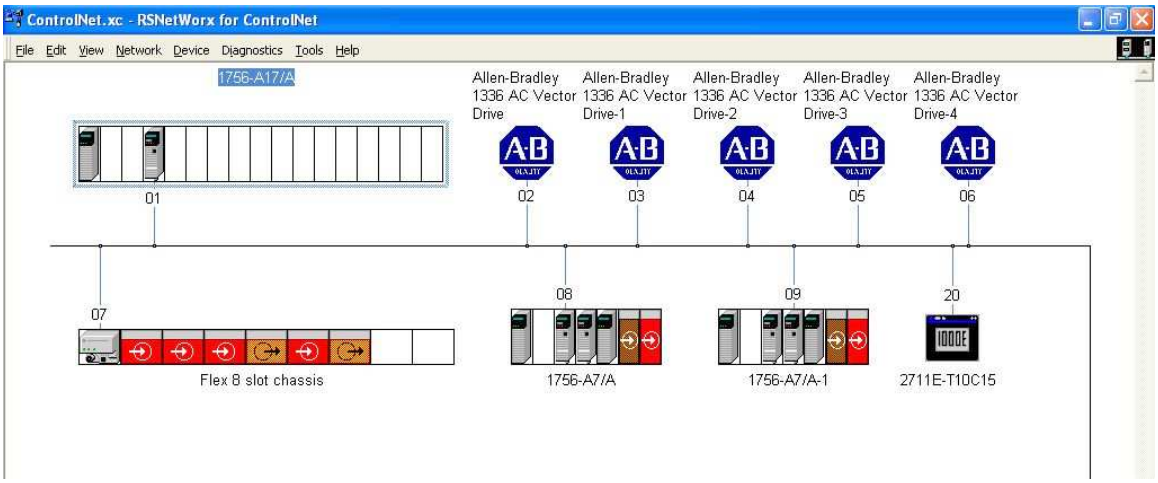

Figure 2.2: Euclid Web Line Hardware Overview

Two three-phase, four-pole induction motors, with 15 HP capacity, are used to drive the unwind and rewind rolls, whereas S-wrap and pull roll rollers are driven by 5 HP induction motors. These motors are coupled with the roller shafts through transmission belts and speed reduction gearboxes. The gear ratio $GR = V_{motor}/V_{roller}$ is equal to 3.795 for the unwind and rewind rolls, 6.82 for the pull roll and 14 for the S-wrap rolls. The characteristics of the motors and transmission systems dictate that the ideal operation velocity of the web line should be less than 500 FPM.

The five AC motors in EWL are driven by five vector control AC 1336T force drives from Rockwell Automation. These AC drives are designed based on the Field Oriented Control technology [13]. The AC drive has the ability to decouple the stator current in each phase into I_d (magnetization current) and I_q (torque current) and control these two currents independently. The I_d current will only generate the flux in the motor and the I_q current will determine the output torque of the motor. Thus, by regulating the I_d and changing the value of I_q at different speed, the AC drive can provide a "DC motor like" performance on AC motor with a speed regulation accuracy up to 0.001% of rated motor speed and torque regulation accuracy of $\pm 5\%$ of rated motor torque [14]. Five encoders are installed on the motor shafts to provide

motor speed feedback. The encoders installed on the unwind and rewind rolls can provide 2048 pulses per revolution, while the encoders installed on the S-wrap and pull roll rollers have a resolution of 1024 PPR. The fact that the velocity regulation accuracy of the AC drive is much better than that of the motor output torque implies that the velocity-controlled tension regulation strategy has an advantage over the torque-controlled tension regulation strategy in an AC motor driven web processing line.

The human machine interface (HMI) touchscreen on the control panel accepts operator's instructions such as line speed, tension references, and provides necessary line status feedback and warning messages. An enable push button and two emergency stop mushroom buttons on the control panel are provided for the operator to operate the web line and ensure safety during experimentation.

Two Controllogix 5000 controllers take charge of all the logic and control tasks of the EWL. One of the controllers (Master) is dedicated to interact with the operator through HMI and push buttons. The Master controller checks if all the safety interlocks have been properly set and the web line initialization has been done, then the master controller will send the line speed and tension references to the other controller (ACDrive), and will continue to monitor the web line's status as well as send line speed and section tension feedback to HMI for display. The Master controller also has several remote digital I/O modules to operate the lateral guides, nip rollers and receive instructions from the push buttons. The ACDrive controller fulfills most of the control algorithms, generates velocity and torque references for the AC motors, maintains the line speed and web tension and collects tension and speed feedback.

In order to regulate the web tension, three load cells have been installed in the EWL. These load cells are located on rollers 7, 13 and 17 to provide tension feedback in the unwind, pull roll and rewind sections, respectively. The sensing range of these load cells is from 0 lbf to 50 lbf, and the tension signal condition module will convert

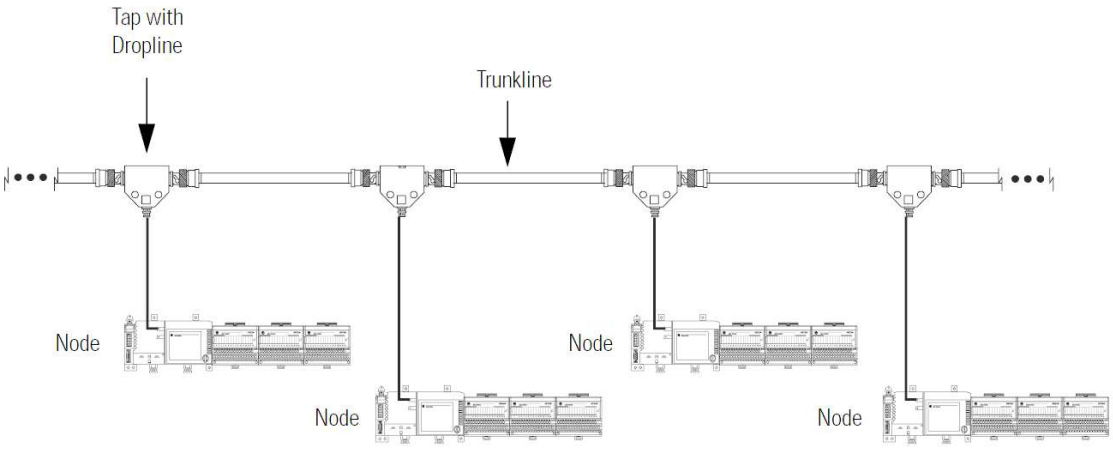

Figure 2.3: ControlNet System Trunkline-Dropline Topology

the web tension to a $0 - 10$ V analog signal. The tension feedback signals are then sent back to the ACDrive controller through an A/D module.

All the communication and data exchange between these two controllers, the HMI and Master controller, the AC drives and the ACDrive controller are accomplished on the ControlNet. The ControlNet is an industrial field communication bus protocol proposed by Rockwell Automation, it can support up to 99 nodes with a 5 Mb/s data transmission speed. More importantly, it is a deterministic network which means it can guarantee that the time-critical data packages arrive at their destinations in the preset time interval, and this feature makes ControlNet especially suitable for industrial control applications. In addition, the high transmission speed and deterministic characteristics of the ControlNet also ensure a fixed sampling rate when the system signals are collected for further analysis. The hardware of the ControlNet network in EWL includes the communication modules in every node, the trunkline cable and the connection taps. The ControlNet in EWL adapts a trunkline-dropline topology as shown in Figure 2.3. The trunkline cable is a coaxial cable from Rockwell Automation. Due to the existence of noise disturbance from the high frequency power switch devices inside the AC drive, fiber cables are used to transmit data between the AC drives and the trunkline in order to improve noise rejection capability.

2.3 The Control System Software

Adaptations have been made to adjust EWL to meet different experimental requirements, and these adjustments on EWL can be summarized as follows:

- Set up the hardware configuration, control algorithms and logic correctly in the controllers.
- Generate user-defined velocity disturbance signals in the control system if required by the experiment.
- Introduce these disturbances into the web handling system as needed by the experiment.
- Collect and analyze the system response data.

Most of these adaptations are done through a set of software from Rockwell Automation: The RSLinx software provides fundamental communication functions between the PC and all the nodes on the ControlNet; the RSLogix 5000 is used to program and debug ControlLogix 5000 controllers; the DriveExecutive is the dedicated software to set up AC 1336T Force drives; finally, the RSNetworx for ControlNet is used to schedule and set up all the ControlNet communication in the control system.

2.3.1 The Configuration and Programming of the Controller

The ControlLogix 5000 controller is an advanced Programmable Logic Controller (PLC) which forms the core of the EWL control system. This high performance industrial controller provides a modularized, flexible, expandable solution to most of the industrial applications. The components of the controller which include CPU modules, communication modules, I/O modules could reside in one or several base racks, and there is no requirement for the location and arrangement sequence of these modules which provides a great hardware configuration flexibility. Furthermore, it is

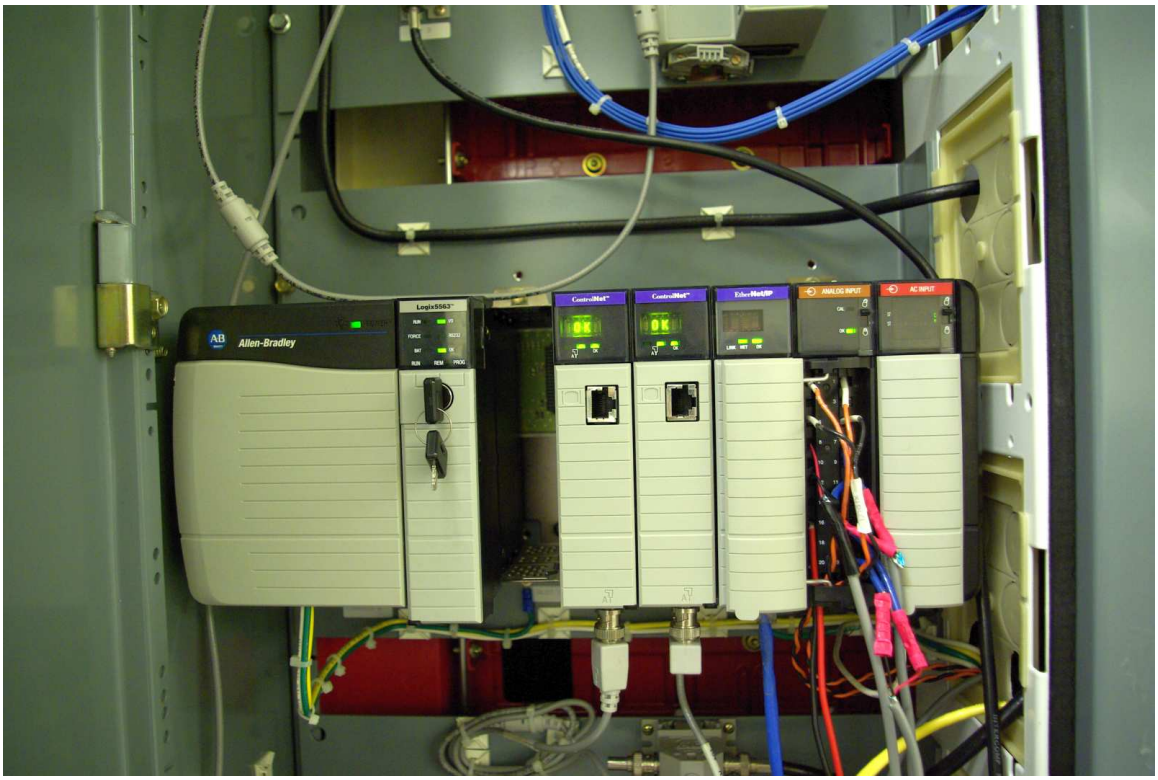

Figure 2.4: ACDrive Controller Rack

possible to expand the capacity of the system by just simply inserting more modules such as another CPU or communication module in the spare rack slots.

A major part of hardware configuration, control algorithm implementation and velocity disturbance generation work are realized in ACDrive controller through RSLogix 5000 software. The ACDrive controller includes a 1756-L63 CPU module (Logix 5563) with 8 MB memory space, two 1756-CNB ControlNet communication modules, one 1756-IF6I 6 channels analog input module and one 1756-IA16 16 points digital input module. A 1756-ENET EtherNet/IP communication module is also located in the rack such that a PC can download/upload programs as well as communication with the controller easily through a standard Internet cable. Figure 2.4 shows the arrangement of these components in the base rack.

When using RSLogix 5000 to program the controller, the hardware configuration as well as the ControlNet topology structure must be set up in the project file first as

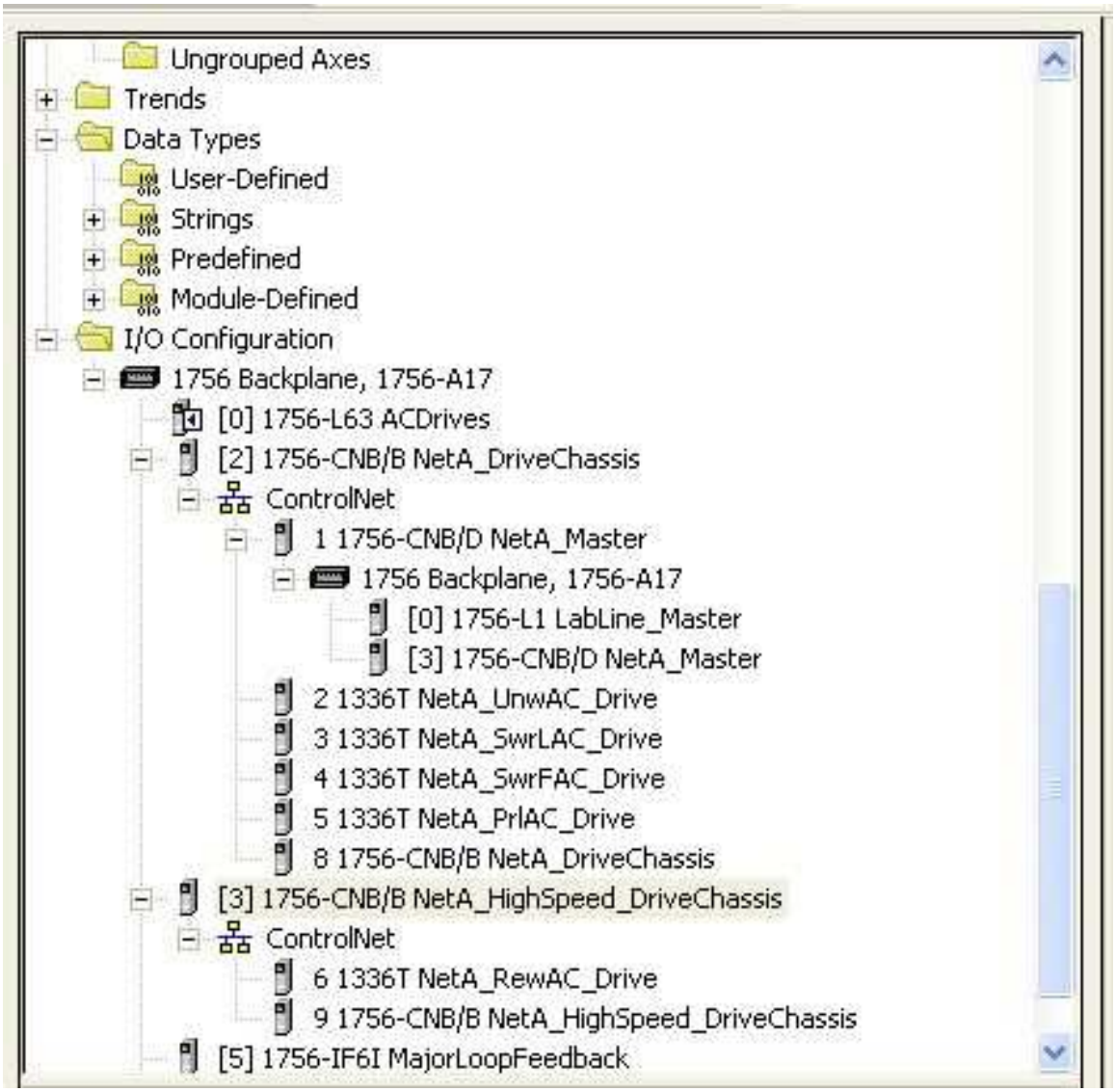

Figure 2.5: Euclid Web Line Hardware Configuration

shown in Figure 2.5. This can be done by selecting "New Module..." command in the right-click menu at proper location in the hardware tree structure and entering the module type and version, reference name, slot number as well as the communication rate if needed [15].

Figure 2.6 shows a typical hierarchy of the ControlLogix controller program. The controller supports three types of tasks: continuous, periodic and event [16]. The continuous task usually includes some background programs which are automatically restarted once they are completed. The periodic task will execute all its code at a preset interval time. Since the controller can guarantee the program running period, the periodic task is especially suitable to realize discrete control algorithm which usually requires a fixed sampling time T_s. The event task is more like an interrupt routine in the PC system, it will only be triggered at the occurrence of an assigned event such as an incoming message or detection of hardware errors. As a multitasking controller, ControlLogix controller also provides a mechanism to avoid the conflicts between tasks by assigning a priority level to each periodic and event task. Meanwhile, the continuous task always has the lowest priority. Tasks with higher priority cause lower priority tasks (and the continuous task) to be suspended so that they can take control and perform their operations; tasks with lower priority wait for higher priority tasks to complete before being given an opportunity to execute; tasks configured at the same priority level are automatically time-sliced switched back and forth till one of the tasks is completed. The Logix 5563 controller supports up to 32 tasks and 15 priority levels.

There could be several programs under one task, and each of these programs can have one and only one "Main" subroutine along with several additional subroutines. The "Main" subroutine must call the other subroutines in order to execute the code in them.

Similar to all other advanced program languages, the programmer can define local

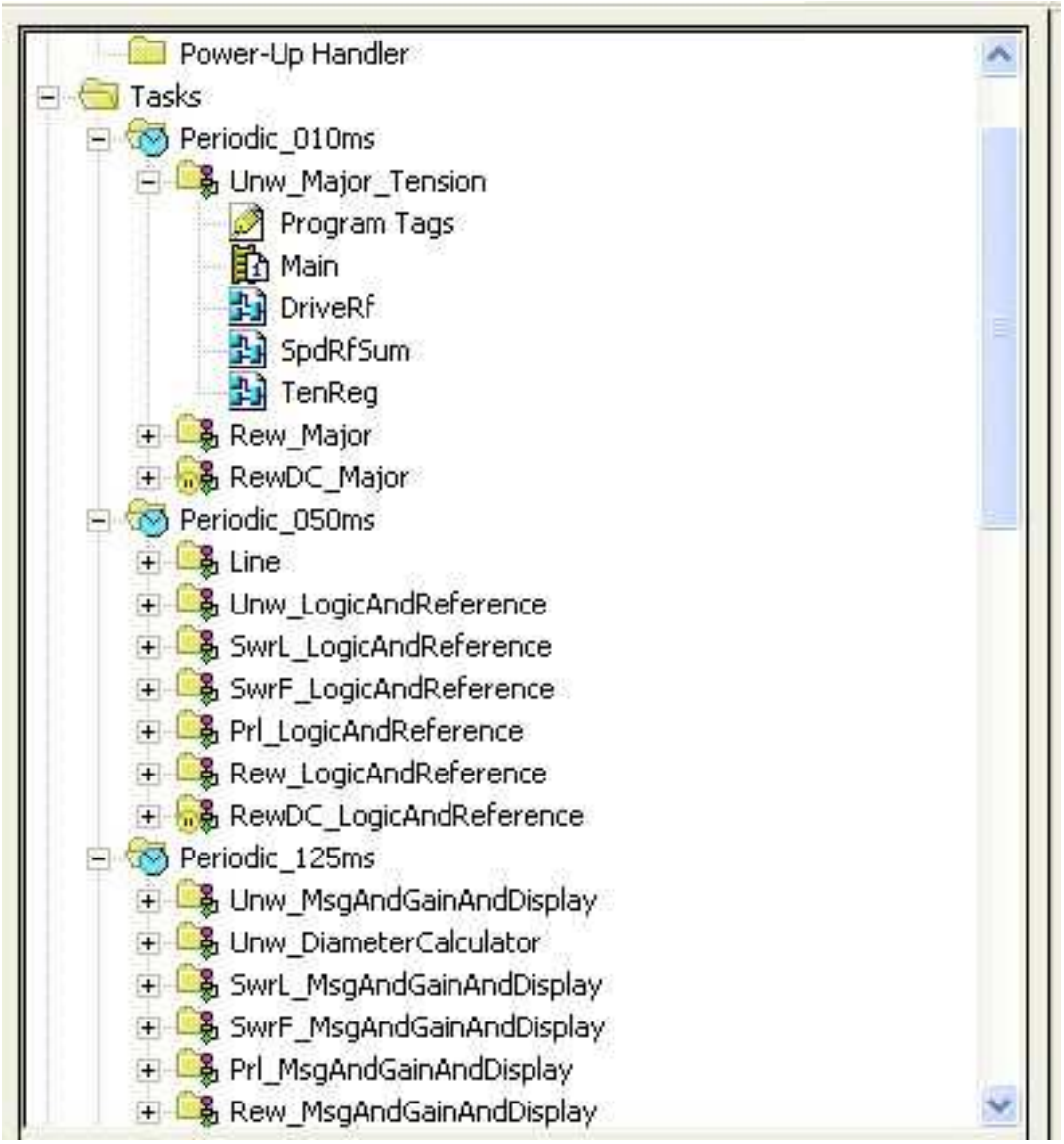

Figure 2.6: Euclid Web Line ACDrive Controller Program Hierarchy

and controller tags (variables) in the program. The local tags can only be accessed in the program to which the tag belongs; on the other hand, the controller tags can be used in any program inside the controller acting as global variables. The local tags are listed in the "Program Tags" in each program while all the controller tags can be found in the "Controller Tags" list.

In the case as shown in Figure 2.6, the ACDrive controller has 3 periodic tasks which have different execution periods ranging from 10 ms to 125 ms, and there is no continuous or event task in the controller. The most critical programs such as the "Unw_Major_Tension", which is used to regulate the unwind section tension and requests the fastest sampling time, reside in the 10 ms periodic task and have the highest priority; the logic check, velocity and tension reference generation programs reside in the 50 ms periodic task and have medium priority; the winder roller diameter and AC drive controller gains calculation programs are in the 125 ms periodic task and have the lowest priority since these programs are not time-critical and the diameters and gains do not need to be updated frequently. Finally, a specified velocity disturbance generation routine (not shown in the figure) has been programmed and located either in 10 ms periodic or 50 ms periodic task depending on the requirements of different experiments. This specified routine can generate sinusoidal velocity disturbances according to the user-defined amplitudes and frequencies.

All routines in the controller can be programmed in four different languages [16]: Ladder Diagram (LD), Function Block Diagram (FBD), Structured Text (ST) and Sequential Function Chart (SFC). For example, the "Main" subroutine of the "Unw_Major_Tension" program under the 10 ms periodic task is written in the LD language, while the other additional subroutines such as "DriveRf" and "TenReg" are all written in the FBD language as shown in Figure 2.6.

2.3.2 Configuration of the ControlNet

The control system of EWL employs a decentralized hardware structure, thus massive data needs to be shared among controllers, drives and HMI in order to operate the web line. For example, the outputs of tension controllers should be sent to unwind and rewind drives so that the web tension can be controlled though changing the velocities of the driven rollers. Also, the measured velocities of five driven motors are expected to be sent back to the ACDrive controller. All of these data exchange activities require a reliable communication path with fixed transmission rate. As the field communication bus, the ControlNet makes this possible, and plays an important role in the control system.

Two important concepts will be introduced first in order to help understand the ControlNet better. The Network Update Time (NUT) is the smallest repetitive time interval in which data can be sent on the ControlNet network. It represents the fastest possible update rate for scheduled data transfers on the network. For example, a network that runs with a 5 ms NUT cannot send data at a rate faster than 5 ms. It can, however, send data at a slower rate. The Requested Packet Interval (RPI) is the update rate specified by the user for a particular piece of data on the network. The RPI cannot be set to a faster rate than the NUT since the network cannot send data at a rate that is faster than NUT.

The configuration of the ControlNet can be completed in two steps [17]. First, add the modules (for ControlLogix controller) or the ControlNet node devices such as the AC drives alone with all other hardware in the RSLogix 5000 project file as mentioned before. Then, assign a unique address number between 1 to 99 as well as the RPI to each of these modules and devices. The programmer can assign different RPIs to these devices as needed by the application. For example, if an RPI of 50 ms is specified to an I/O module, then every 50 ms, this I/O module will send its data to the controller and/or the controller will send its instructions and data to the I/O

module. It should be noted that the faster the RPI, the more network bandwidth is used. So the RPI must be set as fast as necessary to avoid draining the network bandwidth. In the EWL case, the NUT is set to be 5 ms, and since the web tension is quite sensitive to the velocity differences between driven rollers, the RPIs for the five AC drives are either set to be 10 ms or even 5 ms which is the fastest RPI possible so that the network transmission delay and the web tension variation can be reduced to a minimum. Meanwhile, the less time-critical web line status feedback information such as the average line speed, web tension values used for display on the HMI has a relatively larger RPI value equal to 20 ms in order to save the network resource.

After the hardware configuration is done in RSLogix 5000, the project file is downloaded to the controller. Then the RSNetWorx for ControlNet should be used to schedule the network. In this process, the programmer will be required to assign the NUT value of the network, the maximum allowed node address (SMax), the cable media configuration (to calculate the maximum propagation delay between any two nodes) and network name, the software will transfer configuration information to the remote modules, verify and save NUT along with other user-specified network parameters, and will establish a schedule that is compliant with the RPIs and other connection options specified for each module.

Finally, whenever the ControlNet configuration is changed, for example, adding a new node to the network, changing the NUT or RPI value, the two configuration steps above must be redone to reschedule the network and make sure all the nodes in the network can work properly.

2.3.3 Configuration of AC Drives

As the device interfacing with the motor, the 1336T Force AC drive receives the velocity reference from ACDrive controller, and provides a variable voltage, variable frequency AC power supply to the motor so that the velocity of the motor can track

the reference value. The AC drives' regulation performance both in transient and steady state conditions is crucial to the final web line tension and speed control quality. In the experiments, the AC drives are also required to drive the motors to track sinusoidal velocity disturbances so the web line system's frequency response can be investigated without any other new equipment.

The 1336T Force AC drive adopts a typical two-cascaded-control-loop structure along with drive fault detection and logic control, motor protection and autotune functions as shown in Figure 2.7 [14]. The outer velocity loop calculates the difference between the velocity reference and the motor velocity feedback, then a torque reference is generated through a PI controller in order to keep the motor tracking the reference velocity. The motor torque reference is then converted to torque current I_q and controlled by the inner current loop. The AC drive does not allow the user to change its control structure; alternatively, it provides a set of parameters as a configuration interface. By programming these parameters, some of the AC drive functions can be selectively bypassed or activated; thus, the AC drive can adapt itself to different application requirements. There are more than 400 parameters in the drive: parameters 0 through 288 are the parameters for the 1336 Force motor control board, while parameters 300 and above cover the ControlNet adapter board in the AC drive. Some of these parameters are read-only (called "Source") in order to provide the status feedback of the motor and drive itself, such as the motor speed, the motor torque mode status and the stator current value. The other parameters can be changed (called "Sink") accordingly in order to set up the drive which include the gains of the velocity PI controller, the velocity and torque references, the nameplate horsepower and voltage of the motor, the motor winding pole number, the high/low limits on the motor speed and output torque.

These parameters can be accessed through the text-based Human Interface Module (HIM) mounted on the face plate of each drive. Meanwhile, the DriveExecutive

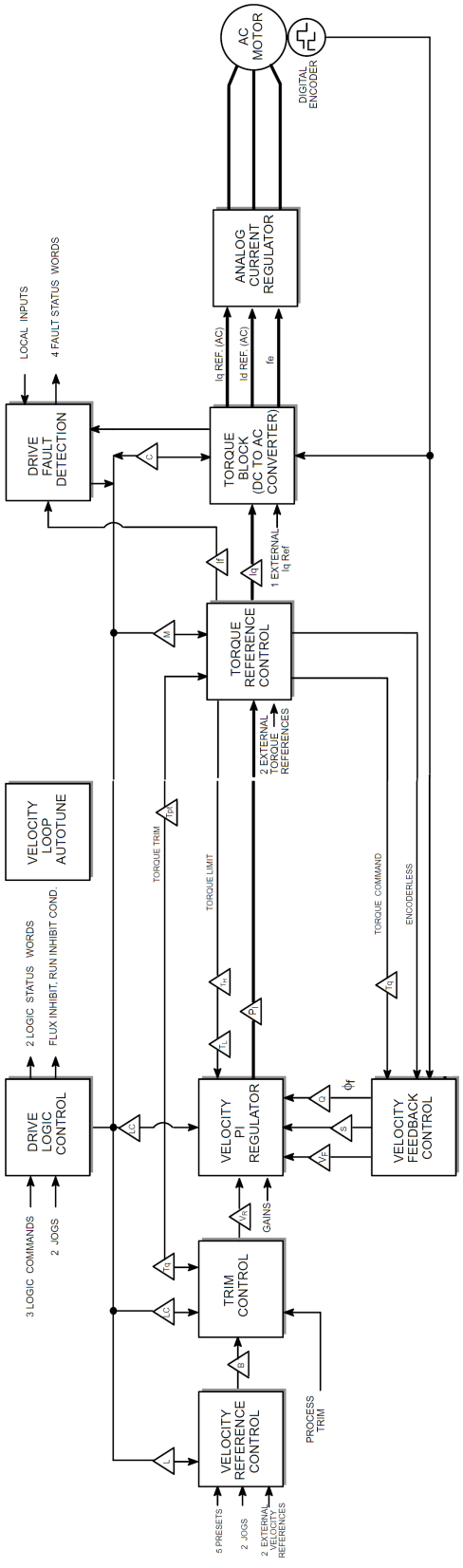

Figure 2.7: 1336T Force AC Drive Function Block Overview

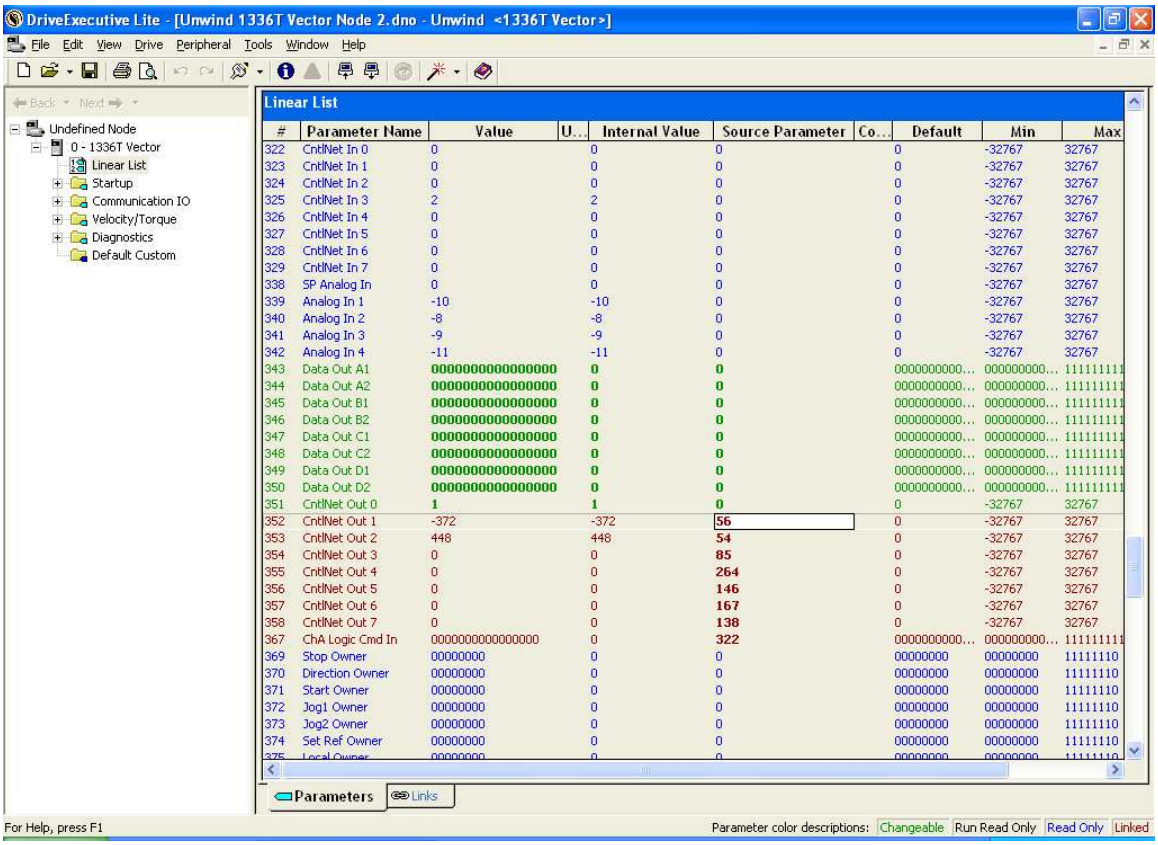

Figure 2.8: DriveExecutive Software Overview

software provides a more convenient method to view, edit and save the parameters on the PC. A screenshot of the software is shown in Figure 2.8. When connecting to the AC drives through ControlNet, DriveExecutive can automatically upload all the parameter values and sort them in different manners for easy access. After configuration and modifications have been done, these new parameter values can be downloaded to the AC drives and put into effect. Meanwhile, a copy of these parameters can be saved in the PC for further use or backup purpose.

The ControlNet adapter board in the drive has the ability to receive and send out 8 parameters on the ControlNet simultaneously, thus it is an efficient way to change the configuration and collect data when the motor is running. As shown in Figure 2.8, the input parameters "CntlNet In" from 322 to 329 will receive the values from the ControlNet every RPI and write them to corresponding linked sink parameters; the output parameters "CntlNet Out" from 352 to 358 will read the values from linked source parameters and send them out on the ControlNet at the rate of predefined RPI. When the EWL is running, the time-varying velocity reference, motor torque reference and the gains of the velocity PI controller are sent to the AC drives from the ACDrive controller; at the same time, the motor speed/current feedback as well as the AC drive/motor running status are sent back to the controller.

2.3.4 Data Collection and Analysis

An online collection, offline analysis data acquisition and interpretation strategy is adopted in experiments. The interested system responses such as the velocities of driven rollers and web tensions were collected and stored online in the ACDrive controller while the experiments were running; the stored data was uploaded later and all further data analysis and interpretation work was done offline in the computer. This strategy takes advantage of the real-time data collection capability of EWL's control system; meanwhile, the data can be analyzed by using existing functions and

techniques of a technical computing software such as MATLAB.

The most widely used data collection method in the control system of EWL is the "Trend" function from RSLogix 5000 software. The trend feature is an efficient tool to collect and visualize multiple system responses (variables) at the same time. A screenshot of a trend is shown in Figure 2.9. In this example trend, concerned system tags which include the motor speed reference and feedback, motor torque and current are collected and plotted in the same trend screen. The trend itself gives an intuitive description of the changes of these tags during the rewind roller's acceleration and deceleration procedure.

Figure 2.10 is the screenshot of configuration interface of the trend in RSlogix 5000. There could be up to 8 tags in one trend, and several trends can be run at the same time, giving a great flexibility in data collection and analysis. The sampling time of the trend can be adjusted according to the application varying from 1 ms to 30 minutes, and the start and stop of the trend can be controlled manually or through the triggers which will automatically run and stop the data collecting based on user-defined conditions. The tag value display format, data point connection type, display time span, legend position as well as plot color can all be customized in this interface for easy data reading. Furthermore, all the collected data can be saved as "TBS" file in order to be viewed again in RSLogix 5000 software or saved as "CSV" format and be imported into MATLAB or Excel for further advanced analysis.

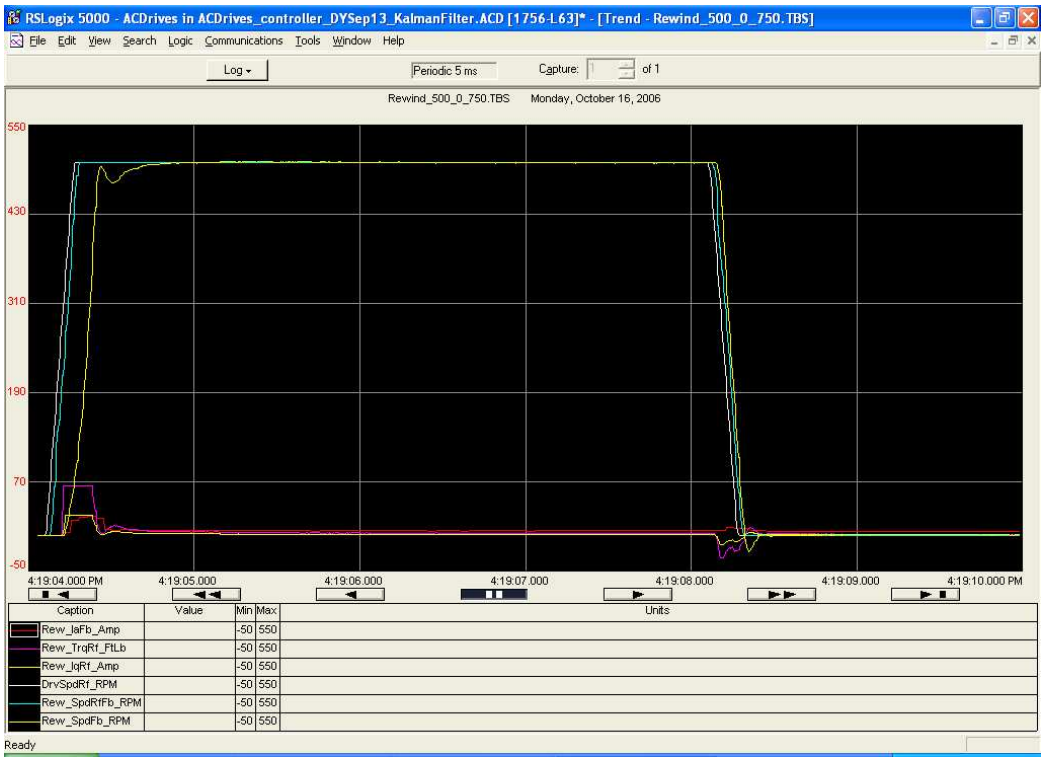

Figure 2.9: Trend in RSLogix 5000

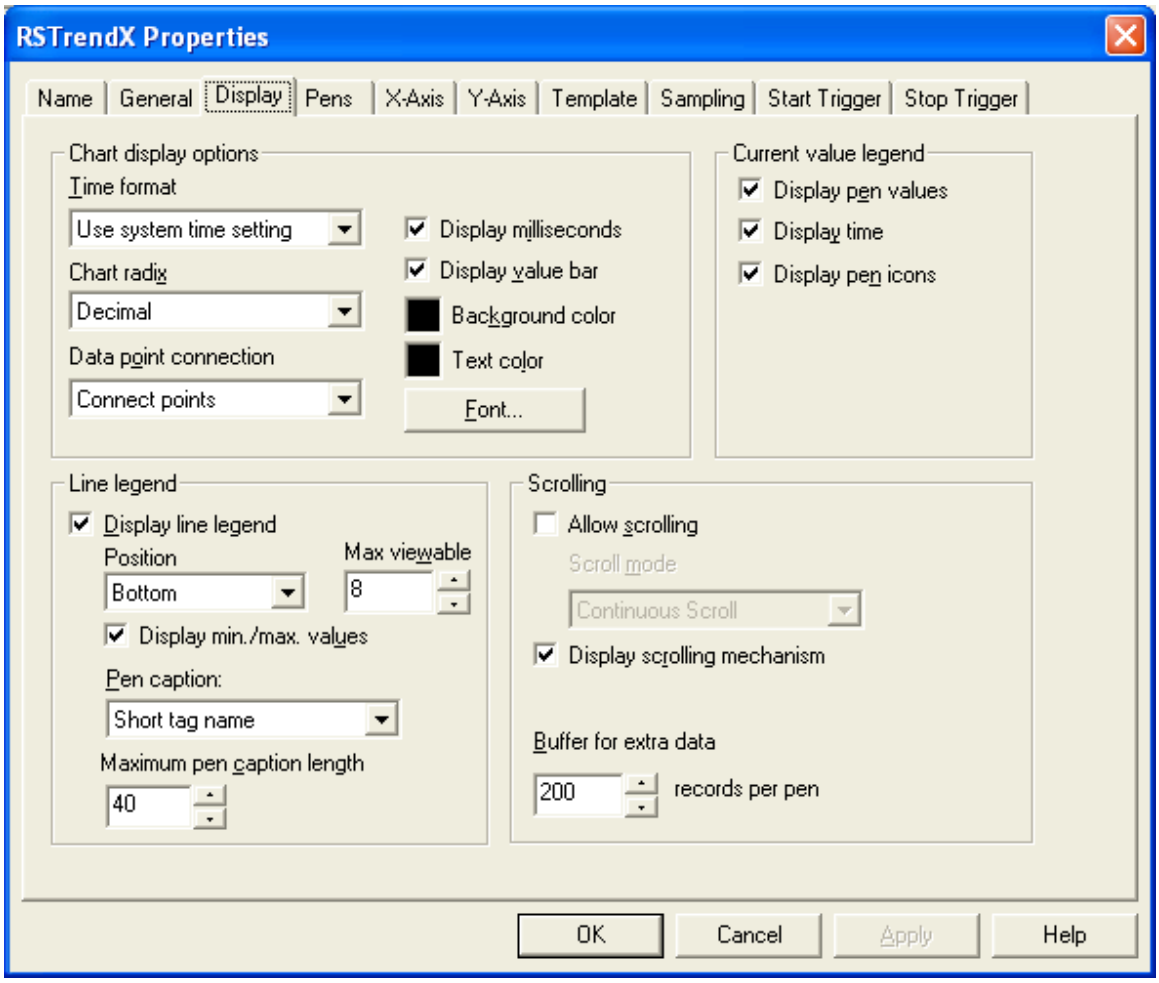

Figure 2.10: Trend Configuration Interface

CHAPTER 3

RESONANT FREQUENCIES OF A SYSTEM OF IDLE ROLLERS AND SPANS IN A WEB LINE

3.1 Introduction

The goal of this chapter is to investigate the resonant frequencies of a system of idle rollers and web spans within two consecutive driven rollers. Of particular interest is the determination of the minimum resonant frequency as a function of the number of idle rollers, web span lengths between the idle rollers, web properties such as the modulus of elasticity and area of cross-section, and inertia and radius of the idle rollers. Any conclusions from the analysis that can provide insights into maximizing the minimum natural frequency by choosing particular web paths or span lengths are of benefit to the web machine designer as well as the control system engineer. Knowledge of the minimum resonant frequency and factors that influence it can assist the machine designer in choosing web paths and/or number of idle rollers between two driven rollers such that the machine induced vibrations do not excite resonances. Further, web tension control systems should be designed such that the bandwidth of the closed-loop system as well as the crossover frequency of the controller are kept below the minimum resonant frequency of the system.

The approach consists of considering a simplified model for web tension between two idle rollers. A state space model of a system of idle rollers and spans is constructed based on the simplified tension model and the web velocity dynamics on the roller. To verify that such a model is capable of predicting resonant frequencies, experiments were conducted for different web paths and number of idle rollers. For

this study, the Euclid Web Line experiment platform was used. The rewind section, between the pull roll and rewind roll, and the pull roll section, between the S-wrap rollers and pull roll, are considered. Due to the presence of a number of idle rollers between the pull roll and rewind roll, it is possible to set up web paths with different idle rollers between them. The experimental results show that the linear model is able to predict the observed tension behavior and the minimum resonant frequency reasonably well. Based on this linear state space model, analytical solutions for the resonant frequencies were obtained for the one and two idle roller cases with unequal web lengths. Numerical analysis for these two cases and web paths with more than two idle rollers has been done. Results from these analyses will be shown and discussed. Further, the case of a number of idle rollers with equal span lengths has been investigated (an accumulator is an example of such a system), and an estimate of the minimum resonant frequency is derived.

3.2 Dynamic Modeling

The modeling process of an idler system between two driven rollers is studied in this section. The nonlinear web tension dynamic equation in a free web span is derived based on the conservation of mass in a control volume. The nonlinear tension dynamic model is simplified to a linear version dedicated to predict the system resonant frequencies. The idler roller motion equation is developed later. The state space equation for an n-idler system is then built up based on the simplified tension dynamics as well as the idler roller dynamics. In order to validate this system model, a series of experiments and simulations have been conducted, and the results suggest that the proposed model is capable of predicting the minimum resonant frequency.

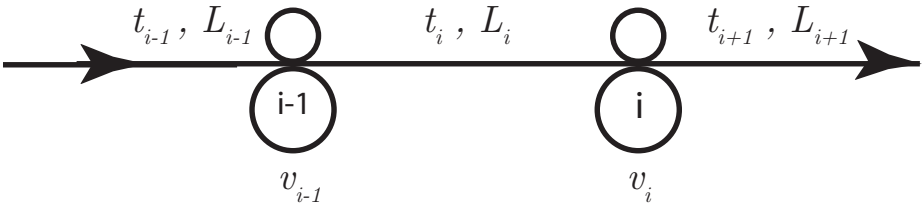

Figure 3.1: A Typical Web Span

3.2.1 Dynamics of Web Tension in a Span

The web between two rollers is called a web span, as shown in Figure 3.1. Modeling of the tension behavior of a web span has been addressed in several studies; examples are [1, 3, 4]. The fundamental idea behind the derivation of the dynamic equation is the conservation of mass in the control volume, which is: at any moment, the variation of the mass of web in the span is equal to the difference between the amount of mass coming from the previous span and the mass leaving the current span to enter the next span. The law of mass conservation can be expressed as:

$$\frac{d}{dt}\int_{x_{i-1}(t)}^{x_i(t)} \rho(x,t)A(x,t)dx = \rho_{i-1}A_{i-1}v_{i-1} - \rho_i A_i v_i \tag{3.1}$$

where $x_{i-1}(t)$ and $x_i(t)$ are the positions of the $(i-1)$-th and i-th roller, ρ is the density of the web, A is web's cross-section area, and v is the web velocity.

Consider the mass of an infinitesimal element of the web in the longitudinal direction:

$$dm = \rho(x,t)A(x,t)dx = \rho_n(x,t)A_n(x,t)dx_n \tag{3.2}$$

where the subscript n denotes the unstretched state, and consider the longitudinal web length relationship between the unstretched and stretched material:

$$dx = (1+\epsilon_x(x,t))dx_n \tag{3.3}$$

where ϵ_x is the web strain at the position x. Substituting (3.3) into (3.2) results in:

$$\frac{\rho(x,t)A(x,t)}{\rho_n(x,t)A_n(x,t)} = \frac{dx_n}{dx} = \frac{1}{1+\epsilon_x(x,t)} \tag{3.4}$$

which can be rearranged as:

$$\rho(x,t)A(x,t) = \frac{\rho_n(x,t)A_n(x,t)}{1+\epsilon_x(x,t)} \tag{3.5}$$

Substituting (3.5) into (3.1):

$$\frac{d}{dt}\int_{x_{i-1}(t)}^{x_i(t)} \frac{\rho_n(x,t)A_n(x,t)}{1+\epsilon_x(x,t)}dx = \frac{\rho_{n_{i-1}}(x,t)A_{n_{i-1}}(x,t)v_{i-1}}{1+\epsilon_{x_{i-1}}(x,t)} - \frac{\rho_{n_i}(x,t)A_{n_i}(x,t)v_i}{1+\epsilon_{x_i}(x,t)} \tag{3.6}$$

Under the assumption that the cross-section area A_n and the density ρ_n of the unstretched material are constants, that is $\rho_n = \rho_{n_{i-1}} = \rho_{n_i}$ and $A_n = A_{n_{i-1}} = A_{n_i}$, (3.6) can be simplified to:

$$\frac{d}{dt}\int_{x_{i-1}(t)}^{x_i(t)} \frac{1}{1+\epsilon_x(x,t)}dx = \frac{v_{i-1}}{1+\epsilon_{x_{i-1}}(x,t)} - \frac{v_i}{1+\epsilon_{x_i}(x,t)} \tag{3.7}$$

Consider that $\epsilon \ll 1$, then $1/(1+\epsilon)$ can be approximated by $(1-\epsilon)$ and hence (3.7) becomes:

$$\frac{d}{dt}\int_{x_{i-1}(t)}^{x_i(t)} (1-\epsilon_x(x,t))dx = v_{i-1}(1-\epsilon_{x_{i-1}}(x,t)) - v_i(1-\epsilon_{x_i}(x,t)) \tag{3.8}$$

Applying the Leibnitz rule for differentiation of integrals:

$$\frac{d}{dt}\int_{\phi(t)}^{\psi(t)} f(x,t)dx = \int_{\phi(t)}^{\psi(t)} \frac{\partial f(x,t)}{\partial t}dx + \frac{d\psi}{dt}f(\psi(t),t) - \frac{d\phi}{dt}f(\phi(t),t) \tag{3.9}$$

and assuming uniform strain throughout the span, that is $\epsilon_x(x,t) = \epsilon_x(t) = \epsilon_{x_i}$, (3.8) can be rewritten in the following way:

$$\frac{d\epsilon_{x_i}}{dt}(x_{i-1}-x_i) + (1-\epsilon_{x_i})\frac{dx_i}{dt} - (1-\epsilon_{x_{i-1}})\frac{dx_{i-1}}{dt} = v_{i-1}(1-\epsilon_{x_{i-1}}) - v_i(1-\epsilon_{x_i}) \tag{3.10}$$

which can be simplified as:

$$\frac{d\epsilon_{x_i}}{dt} = \frac{v_i(1-\epsilon_{x_i}) - v_{i-1}(1-\epsilon_{x_{i-1}}) + (1-\epsilon_{x_i})\dot{x}_i - (1-\epsilon_{x_{i-1}})\dot{x}_{i-1}}{x_i - x_{i-1}} \tag{3.11}$$

Equation (3.11) is the dynamic equation for web strain in a span.

Depending on the property of the web, it is possible to introduce a constitutive relationship between web strain and web tension. Assuming the web to be elastic,

Hooke's law ($t = EA\epsilon$) can be used to describe the relationship between web tension and strain, and (3.11) can be simplified to form the dynamic equation for web tension in the span:

$$\dot{t}_i = \frac{v_i(EA - t_i) - v_{i-1}(EA - t_{i-1}) + (EA - t_i)\dot{x}_i - (EA - t_{i-1})\dot{x}_{i-1}}{x_i - x_{i-1}} \tag{3.12}$$

Equation (3.12) is the most comprehensive form for the web span tension dynamics, in fact, it also includes the hypothesis that both the span's end rollers are free to move (notice the $\dot{x}_i$ and $\dot{x}_{i-1}$ terms).

In the case that both of the end rollers are stationary, that is $\dot{x}_i = \dot{x}_{i-1} = 0$, and considering $x_i - x_{i-1} = L_i$, (3.12) becomes:

$$\begin{aligned} \dot{t}_i &= \frac{v_i(EA - t_i) - v_{i-1}(EA - t_{i-1})}{L_i} \\ &= \frac{EA}{L_i}(v_i - v_{i-1}) + \frac{1}{L_i}(v_{i-1}t_{i-1} - v_i t_i) \end{aligned} \tag{3.13}$$

Equation (3.13) is the web tension model between two fixed rollers and will be used in the rest of the thesis.

3.2.2 Simplified Web Span Tension Equation Between Two Idlers

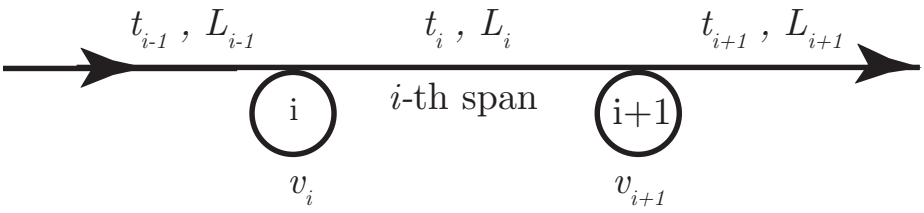

Figure 3.2: i-th Span in an Idler System

For the ith span in an idler system shown in Figure 3.2, applying the web tension equation (3.13), the web tension dynamics between two idlers is:

$$L_i\dot{t}_i = EA(v_{i+1} - v_i) + (t_{i-1}v_i - t_i v_{i+1}) \tag{3.14}$$

The nonlinear web span tension dynamics can be then linearized around given reference velocity and tension values by defining the perturbations around the reference

value: $V_i = v_i - v_r$ and $T_i = t_i - t_r$, where v_r and t_r are velocity and tension references, respectively. Substitution of these into the nonlinear web tension dynamics and using $\dot{t}_r = \dot{v}_r = 0$ gives

$$L_i\dot{T}_i = EA(V_{i+1} - V_i) + t_r(V_i - V_{i+1}) + v_r(T_{i-1} - T_i) + T_{i-1}V_i - T_iV_{i+1} \tag{3.15}$$

Ignoring the second-order perturbation terms (the last two terms)

$$L_i\dot{T}_i = (EA - t_r)(V_{i+1} - V_i) + v_r(T_{i-1} - T_i) \tag{3.16}$$

Notice $\dot{T}_i = \dot{t}_i$, $V_{i+1} - V_i = v_{i+1} - v_i$ and $T_{i+1} - T_i = t_{i+1} - t_i$, the linearized dynamics can be written as

$$L_i\dot{t}_i = (EA - t_r)(v_{i+1} - v_i) + v_r(t_{i-1} - t_i) \tag{3.17}$$

Since the quantity EA is typically much larger than the reference tension t_r and reference velocity v_r, the following simplified model of web tension is considered for the prediction of resonant frequencies for a system of idle rollers:

$$L_i\dot{t}_i = EA(v_{i+1} - v_i) \tag{3.18}$$

Note that this model does not consider web strain transport from upstream to downstream spans and hence is not suitable for control system design; one has to consider the nonlinear model (3.14) or the full linearized model (3.17) for control design purposes. But the simplified model given by (3.18) is capable of predicting resonant frequencies (data from a series of experiments which are shown later supports this) and allows for the ease of computation and analysis of the system minimum resonant frequency.

3.2.3 Idle Roller Model

The angular velocity dynamics of the i-th idle roller in the system with the web under tension on either side of it can be obtained by applying Newton's second law as

$$J_i\dot{\omega}_i = R_i(t_i - t_{i-1}) \tag{3.19}$$

Assuming that the web is not slipping on the roller, the web velocity on the i-th roller is given by

$$v_i = R_i \omega_i \tag{3.20}$$

Substitution of (3.20) into (3.19) and simplification gives

$$\frac{J_i}{R_i^2} \dot{v}_i = t_i - t_{i-1} \tag{3.21}$$

3.2.4 Idler System Dynamic Model

The following simplified model forms the basis for subsequent idler system analysis:

$$\dot{t}_i = \frac{EA}{L_i} (v_{i+1} - v_i) \tag{3.22}$$

$$\dot{v}_i = \frac{1}{m_i} (t_i - t_{i-1}) \tag{3.23}$$

where $m_i = J_i / R_i^2$ is the equivalent mass of the i-th idler roller.

Governing equations for an idler system consisting of any number of idlers and spans can be obtained by recursively applying the above equations to every web span and idler. For example, the dynamic equation for a system consisting of one idle roller and two web spans between the pull roll and rewind roll is given by

$$\underbrace{\begin{bmatrix} \dot{t}_0 \\ \dot{v}_1 \\ \dot{t}_1 \end{bmatrix}}_{\dot{\mathbf{x}}} = \underbrace{\begin{bmatrix} 0 & \frac{EA}{L_0} & 0 \\ -\frac{1}{m_1} & 0 & \frac{1}{m_1} \\ 0 & -\frac{EA}{L_1} & 0 \end{bmatrix}}_{\mathbf{A}_1} \underbrace{\begin{bmatrix} t_0 \\ v_1 \\ t_1 \end{bmatrix}}_{\mathbf{x}} + \underbrace{\begin{bmatrix} -\frac{EA}{L_0} & 0 \\ 0 & 0 \\ 0 & \frac{EA}{L_1} \end{bmatrix}}_{\mathbf{B}_1} \begin{bmatrix} v_p \\ v_w \end{bmatrix} \tag{3.24}$$

In the above system, the state vector is $\mathbf{x} = [t_0, v_1, t_1]^\top$, the pull roll velocity, v_p, and the rewind velocity, v_w, are controlled variables and thus are treated as system inputs. Meanwhile, for a two-idler system with state vector as $\mathbf{x} = [t_0, v_1, t_1, v_2, t_2]^\top$,

the system matrix is given by

$$\mathbf{A}_2 = \begin{bmatrix} 0 & \frac{EA}{L_0} & 0 & 0 & 0 \\ -\frac{1}{m_1} & 0 & \frac{1}{m_1} & 0 & 0 \\ 0 & -\frac{EA}{L_1} & 0 & \frac{EA}{L_1} & 0 \\ 0 & 0 & -\frac{1}{m_2} & 0 & \frac{1}{m_2} \\ 0 & 0 & 0 & -\frac{EA}{L_2} & 0 \end{bmatrix} = \begin{bmatrix} & & & 0 & 0 \\ & \mathbf{A}_1 & & 0 & 0 \\ & & & \frac{EA}{L_1} & 0 \\ 0 & 0 & -\frac{1}{m_2} & 0 & \frac{1}{m_2} \\ 0 & 0 & 0 & -\frac{EA}{L_2} & 0 \end{bmatrix}$$

Similarly, for a three-idler system with state vector $\mathbf{x} = [t_0, v_1, t_1, v_2, t_2, v_3, t_3]^\top$, the system matrix is

$$\mathbf{A}_3 = \begin{bmatrix} 0 & \frac{EA}{L_0} & 0 & 0 & 0 & 0 & 0 \\ -\frac{1}{m_1} & 0 & \frac{1}{m_1} & 0 & 0 & 0 & 0 \\ 0 & -\frac{EA}{L_1} & 0 & \frac{EA}{L_1} & 0 & 0 & 0 \\ 0 & 0 & -\frac{1}{m_2} & 0 & \frac{1}{m_2} & 0 & 0 \\ 0 & 0 & 0 & -\frac{EA}{L_2} & 0 & \frac{EA}{L_2} & 0 \\ 0 & 0 & 0 & 0 & -\frac{1}{m_3} & 0 & \frac{1}{m_3} \\ 0 & 0 & 0 & 0 & 0 & -\frac{EA}{L_3} & 0 \end{bmatrix} = \begin{bmatrix} & & & & & 0 & 0 \\ & & & & & 0 & 0 \\ & & \mathbf{A}_2 & & & 0 & 0 \\ & & & & & 0 & 0 \\ & & & & & \frac{EA}{L_2} & 0 \\ 0 & 0 & 0 & 0 & -\frac{1}{m_3} & 0 & \frac{1}{m_3} \\ 0 & 0 & 0 & 0 & 0 & -\frac{EA}{L_3} & 0 \end{bmatrix}$$

One can build up the system matrix from lower-order system matrices as more idle rollers are added. In the system matrix of an n-idler system, $\mathbf{A}_n$, the system matrix of $(n-1)$-idler system, which is $\mathbf{A}_{n-1}$, appears in block-diagonal form as shown above. Therefore, one can recursively write down the system matrix for any number of idle rollers and spans. For a system with n idlers, consisting of $n+1$ web spans, the size of the system matrix is $(2n+1) \times (2n+1)$. The system matrix is a tridiagonal matrix with all its eigenvalues (complex conjugate pairs) on the imaginary axis of the complex plane with one of those at the origin. The zero eigenvalue corresponds to the so-called "rigid body" mode of the system. The resonant frequencies of the idler system are equal to the modulus of all non-zero imaginary-axis eigenvalues of the system matrix. Therefore, to study the resonant frequencies, one needs to analytically obtain the

eigenvalues of the system matrix. Closed-form analytical solutions can be obtained for one- and two-idler systems in a form suitable for analysis. Although closed-form solutions for systems consisting of a larger number of idlers can be obtained using symbolic computational tools, the expressions for resonant frequencies can be quite complicated. Thus, it is difficult to ascertain from the symbolic expressions which one corresponds to the minimum resonant frequency. Even when it is possible to distinguish the minimum resonant frequency, it is difficult to obtain meaningful conclusions on its dependence on physical parameters such as web modulus, span lengths, and roller inertias. For systems consisting of more than two idle rollers, one typically has to resort to numerical analysis.

3.2.5 Validity of the Simple Idler System Dynamic Model to Predict Resonant Frequencies

To verify the simple system model given by equations (3.22) and (3.23), frequency response experiments were conducted on the Euclid Web Line (EWL) for the following systems: one path with 5 idlers between the S-wrap roll and pull roll and two paths with 5 and 7 idlers, respectively, between the pull roll and rewind roll. The pull roll velocity reference v_{pr} is treated as the system input variable, and web tension t is taken as the output variable. The web tension in each section is measured by a load cell. Web tension response data was obtained by sweeping a sinusoidal input containing various frequencies.

The pull roll was in the velocity regulation mode and the following reference velocity v_{pr} was considered:

$$v_{pr} = \bar{v}_r + M(\sin 2\pi\nu_1 t + \sin 2\pi\nu_2 t + \cdots + \sin 2\pi\nu_n t) \tag{3.25}$$

where $\bar{v}_r$ denotes a constant base speed, M is the amplitude of the disturbance, and $\nu_1, \nu_2, \ldots, \nu_n$ are the disturbance input frequencies. The velocity PI controller for the

pull roll was chosen as:

$$C_{pv}(s) = \frac{k_{ps}(s + \omega_{ld})}{s} \tag{3.26}$$

where $k_{ps} = J_p k_{rf}$, $k_{rf} = 40$ and J_p is the pull roll total inertia reflected to the motor side. Also, $\omega_{ld} = k_{rf}/4\zeta^2$, where $\zeta = 1.1$ is the damping ratio of the system.

The control strategy for the rewind roll is a cascaded tension-velocity controller. The inner velocity loop controller is

$$C_{rv}(s) = \frac{k_{ps}(s + \omega_{ld})}{s} \tag{3.27}$$

where $k_{ps} = J_r k_{rf}$ where $k_{rf} = 15$ and J_r is the rewind roll total inertia reflected to the motor side. Also, $\omega_{ld} = k_{rf}/4\zeta^2$, where $\zeta = 1.1$ is the damping ratio of the system.

For the outer tension control loop, a de-tuned PI controller with very low gains was chosen to avoid web breakage. The tension controller can be written as

$$C_{rt}(s) = 2\left(\frac{s+3}{s}\right) \tag{3.28}$$

Three web paths were considered as shown in Figures 3.3, 3.4, 3.5 shown at the end of this chapter. The corresponding span lengths for the three paths are shown in tables below the figures. The inertia J_i and radius R_i of the idle rollers are equal to 0.069874 lb-ft^2 and 0.125 ft, respectively. The web material used in the experimentation is Tyvek with the value of EA equal to 2000 lbf. The pull roll base speed $\bar{v}_r$ was fixed at 150 FPM, the disturbance amplitude M was 5 FPM, and the disturbance frequencies ν_i were chosen from 1 Hz to 19 Hz in steps of 1 Hz. Additional non-integer disturbance frequency components were added in order to get tension response data close to a resonant frequency.

At the beginning of the experiment, the web line was running at the steady base speed $\bar{v}_r$, then velocity disturbance components were injected into the system through the pull roll. Web tensions were measured by load cells in each section. Computer

simulations with the state space models for the same web paths were conducted, where the pull roll velocity feedback v_p is used as system input. To compare the experimental data with simulation data, FFT of each set of data was obtained.

Comparison of the tension FFT data from experiments and model simulations for the three cases are shown in Figures 3.6, 3.7, and 3.8. Note the DC components in the experiment and simulation results have been filtered out to emphasize the frequency response part. It is evident that the model simulation is able to capture the minimum resonant frequencies observed in all three experiments, that is 6.2 Hz for the rewind section five-idler system, 4.5 Hz for the rewind section seven-idler system and 5.6 Hz for the pull roll five-idler configuration, respectively.

3.2.6 Full Linearized Idler System Model

In subsection (3.2.4), a simplified idler system dynamic model is formed. Even though the experimental results in subsection (3.2.5) have shown that this model can predict an idler system's minimum resonant frequency, it can be seen that the resonant frequencies derived from this simplified model are independent of web line reference speed v_r and tension t_r. In order to reveal the potential relationship between these parameters and system resonant frequencies, it is desired to develop an idler system model based on more universal web tension dynamics.

The full linearized web tension equation (3.17) can be rearranged as:

$$\dot{t}_i = \frac{v_r t_{i-1}}{L_i} - \frac{(EA - t_r)}{L_i} v_i - \frac{v_r t_i}{L_i} + \frac{(EA - t_r)}{L_i} v_{i+1} \tag{3.29}$$

In the following, Equation (3.29) will replace the simplified tension dynamics (3.22) in idler system models. For a two-idler system with state vector as $\mathbf{x} = [t_0, v_1, t_1, v_2, t_2]^\top$,

the system matrix $\mathbf{A}_2^F$ based on full linearized tension dynamics is given by

$$\mathbf{A}_2^F = \begin{bmatrix} -\frac{v_r}{L_0} & \frac{EA-t_r}{L_0} & 0 & 0 & 0 \\ -\frac{1}{m_1} & 0 & \frac{1}{m_1} & 0 & 0 \\ \frac{v_r}{L_1} & -\frac{EA-t_r}{L_1} & -\frac{v_r}{L_1} & \frac{EA-t_r}{L_1} & 0 \\ 0 & 0 & -\frac{1}{m_2} & 0 & \frac{1}{m_2} \\ 0 & 0 & \frac{v_r}{L_2} & -\frac{EA-t_r}{L_2} & -\frac{v_r}{L_2} \end{bmatrix}$$

Similarly, for a three-idler system with state vector $\mathbf{x} = [t_0, v_1, t_1, v_2, t_2, v_3, t_3]^\top$, the system matrix is

$$\mathbf{A}_3^F = \begin{bmatrix} -\frac{v_r}{L_0} & \frac{EA-t_r}{L_0} & 0 & 0 & 0 & 0 & 0 \\ -\frac{1}{m_1} & 0 & \frac{1}{m_1} & 0 & 0 & 0 & 0 \\ \frac{v_r}{L_1} & -\frac{EA-t_r}{L_1} & -\frac{v_r}{L_1} & \frac{EA-t_r}{L_1} & 0 & 0 & 0 \\ 0 & 0 & -\frac{1}{m_2} & 0 & \frac{1}{m_2} & 0 & 0 \\ 0 & 0 & \frac{v_r}{L_2} & -\frac{EA-t_r}{L_2} & -\frac{v_r}{L_2} & \frac{EA-t_r}{L_2} & 0 \\ 0 & 0 & 0 & 0 & -\frac{1}{m_3} & 0 & \frac{1}{m_3} \\ 0 & 0 & 0 & 0 & \frac{v_r}{L_3} & -\frac{EA-t_r}{L_3} & -\frac{v_r}{L_3} \end{bmatrix}$$

$$= \begin{bmatrix} & & & & 0 & 0 \\ & & & & 0 & 0 \\ & \mathbf{A}_2^F & & & 0 & 0 \\ & & & & 0 & 0 \\ & & & & \frac{EA-t_r}{L_2} & 0 \\ 0 & 0 & 0 & 0 & 0 & \frac{1}{m_3} \\ 0 & 0 & 0 & 0 & -\frac{1}{m_3} & 0 \\ 0 & 0 & 0 & 0 & \frac{v_r}{L_3} & -\frac{EA-t_r}{L_3} & -\frac{v_r}{L_3} \end{bmatrix}$$

In this way, one can build up the system matrix from lower-order system matrices as more idle rollers are added. For an n-idler system, the size of the system matrix,

$\mathbf{A}_n^F$, is $(2n+1)\times(2n+1)$, and $\mathbf{A}_n^F$ contains the reference values v_r and t_r. Compared to the simplified system matrix $\mathbf{A}_n$, $\mathbf{A}_n^F$ has all its eigenvalues (complex conjugate pairs) on the left half-plane of the complex plane with one of those on the real axis. The undamped resonant frequencies of the idler system are equal to the modulus of all complex conjugate eigenvalues of the system matrix, and the damped resonant frequencies are equal to the absolute value of the imaginary part of complex conjugate eigenvalues.

In the following, the minimum resonant frequency of the rewind section five-idler system derived from the full linearized model is compared with the one previously obtained from simplified idler system model. It has been shown in subsection (3.2.5) that the minimum resonant frequency for this five-idler system is 6.2 Hz which corresponds to a pair of $\mathbf{A}_5$'s eigenvalues at $\pm 38.77i$ in the complex plane. Choosing $v_r = 150$ FPM and $t_r = 20$ lbf, the corresponding eigenvalues of system matrix $\mathbf{A}_5^F$ can be calculated with the value of $0.22 \pm 38.57i$, and the undamped minimum resonant frequency is approximately equal to 6.14 Hz. For a high speed web process line, increasing the reference velocity v_r to 3000 FPM and using the same other system parameters, the corresponding system eigenvalues and minimum resonant frequency are slightly changed to $-4.36 \pm 38.17i$ and 6.1 Hz, respectively. Similarly, when the reference tension t_r is equal to 100 lbf with all other parameters unchanged, the system eigenvalues and minimum resonant frequency are shifted to $-0.22 \pm 37.78i$ and 6.0 Hz. Thus, compared to the simplified idler system model, the full linearized system model and web line reference parameters only introduce some damping effects into the system which move system eigenvalues from the imaginary axis to the left half-plane of the complex plane but do not change their values significantly.

All of these analyses above show that the simplified model can predict an idler system's minimum resonant frequency as well as the full linearized model, the difference between prediction results from these two models is trivial and can be ignored in

real applications. Due to the simplicity (tridiagonal form) of $\mathbf{A}_n$ which makes itself easy to analyze and compute, the simplified idler system model will be used in the following analytical and numerical analyses.

3.3 Analytical Solutions for One- and Two-Idler Systems

Due to the complexity of analytically solving for the system resonant frequencies (modulus of the complex-conjugate eigenvalues of the system matrices), one- and two-idler systems will be discussed here to highlight the process.

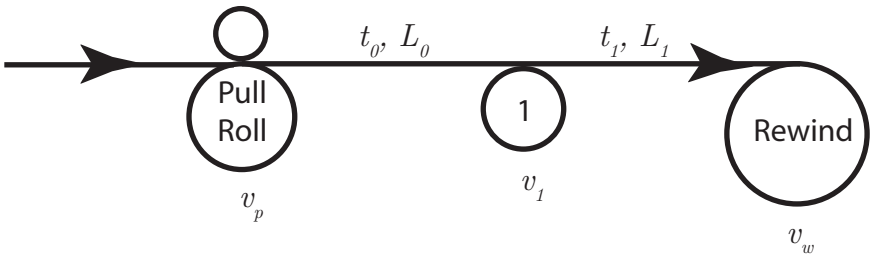

Figure 3.9: One-Idler System

For the one-idler system shown in Figure 3.9, the resonant frequencies are:

$$\begin{aligned} f_0 &= 0 \\ f_1 &= \frac{1}{2\pi}\sqrt{\frac{EA}{m}} \cdot \sqrt{\frac{1}{L_0} + \frac{1}{L_1}} \end{aligned} \tag{3.30}$$

where f_0 corresponds to the rigid-body mode of the system and f_1 is the minimum resonant frequency. Observe that an increase in L_0 and/or L_1 results in a decrease in the minimum resonant frequency f_1. Assuming the total span length $L_0 + L_1 = 2L$, with a constant L, among all combinations of L_0 and L_1 satisfying this assumption, the minimum resonant frequency is of the smallest value when $L_0 = L_1 = L$, and it is given by $f_{1\min} = (1/2\pi)\sqrt{2EA/mL}$.

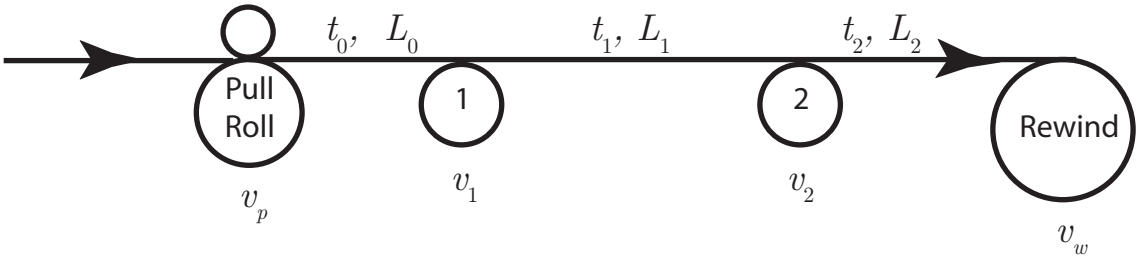

Figure 3.10: Two-Idler System

For the two-idler system shown in Figure 3.10, the system resonant frequencies are:

$$f_0 = 0$$

$$f_1 = \frac{1}{2\pi}\sqrt{\frac{EA}{m}} \cdot \sqrt{\frac{-\sqrt{L_1^2(L_2 - L_0)^2 + 4(L_0L_2)^2} + L_0L_1 + 2L_0L_2 + L_1L2}{2L_0L_1L_2}} \tag{3.31}$$

$$f_2 = \frac{1}{2\pi}\sqrt{\frac{EA}{m}} \cdot \sqrt{\frac{\sqrt{L_1^2(L_2 - L_0)^2 + 4(L_0L_2)^2} + L_0L_1 + 2L_0L_2 + L_1L2}{2L_0L_1L_2}} \tag{3.32}$$

The minimum resonant frequency is f_1 for all L_0, L_1, and L_2. Also, if the end span lengths are the same, that is, $L_0 = L_2 = L$, the minimum resonant frequency is independent of L_1 and is given by

$$f_1 = \frac{1}{2\pi}\sqrt{\frac{EA}{mL}} \tag{3.33}$$

Therefore, if the end span lengths are the same in a three-span system, the middle span length (L_1) can be arbitrarily increased without affecting the minimum resonant frequency. Also, from the above expressions for resonant frequencies, it is clear that interchanging the values of L_0 and L_2 does not change the resonant frequencies.

3.4 Numerical Analysis

It is generally difficult to obtain useful expressions for the resonant frequencies if the number of idlers is more than two. Even if the expressions for resonant frequencies can be found, it may not be possible to identify the minimum one. Numerical analysis

of the resonant frequencies, by varying dependent physical quantities such as span lengths, roller inertias, and modulus of elasticity, can provide some insights into the behavior of the minimum resonant frequency as a function of these physical quantities. In the following, the minimum resonant frequencies of the two-, three-, and four-idler systems are numerically analyzed as a function of the span lengths and modulus of elasticity. For simplicity, all the idlers are treated as identical with inertia $J = 0.069874$ lbm-ft^2 (=0.00217 lbf-ft-s^2) and radius $R = 0.125$ ft, which results in the equivalent mass, $m = J/R^2 = 4.4719$ lbm (=0.1389 lbf-ft^{-1}-s^2). Further, except for the last numerical simulation, EA is taken to be 2000 lbf.

3.4.1 Two-Idler System

Numerical simulations of the model for the two-idler system are performed using the following procedure:

1. Choose L_0 and L_2 such that $L_0 + L_2 = 10$ ft.
2. Choose the middle span length as $L_1 = 50$ ft.
3. Increase L_0 from 0.1 ft to 9.9 ft in steps of 0.1 ft and correspondingly decrease L_2 from 9.9 ft to 0.1 ft to comply with step 1.
4. For each pair of L_0 and L_2, solve the system matrix $\mathbf{A}_2$ for the minimum resonant frequency f_1, and plot the trajectory of f_1 in 3D space as a function of L_0 and L_2.
5. Repeat the above steps for two other L_1 values, 5 ft and 10 ft.

The trajectories of minimum resonant frequency as a function of L_1 and L_2 are shown in Figure 3.11. Figure 3.11 verifies the fact that when $L_0 = L_2$, the minimum resonant frequency takes the same value irrespective of the span length L_1; that is, in the

figure, $L_0 = L_2 = 5$ ft is a single point for all L_1. Figure 3.11 also reveals some other guidelines on choosing L_0 and L_1 if the middle span length L_1 is fixed:

1. If $L_0 + L_2 = 2L < L_1$, choosing $L_0 = L_2 = L$ will maximize the minimum resonant frequency.

2. If $L_0 + L_2 = L_1$, any combination of L_0 and L_1 will result in the same minimum resonant frequency.

3. If $L_0 + L_2 = 2L > L_1$, the minimum resonant frequency can be increased by increasing $|L_0 - L_2|$. The minimum value of f_1 will be attained for $L_0 = L_2 = L$.

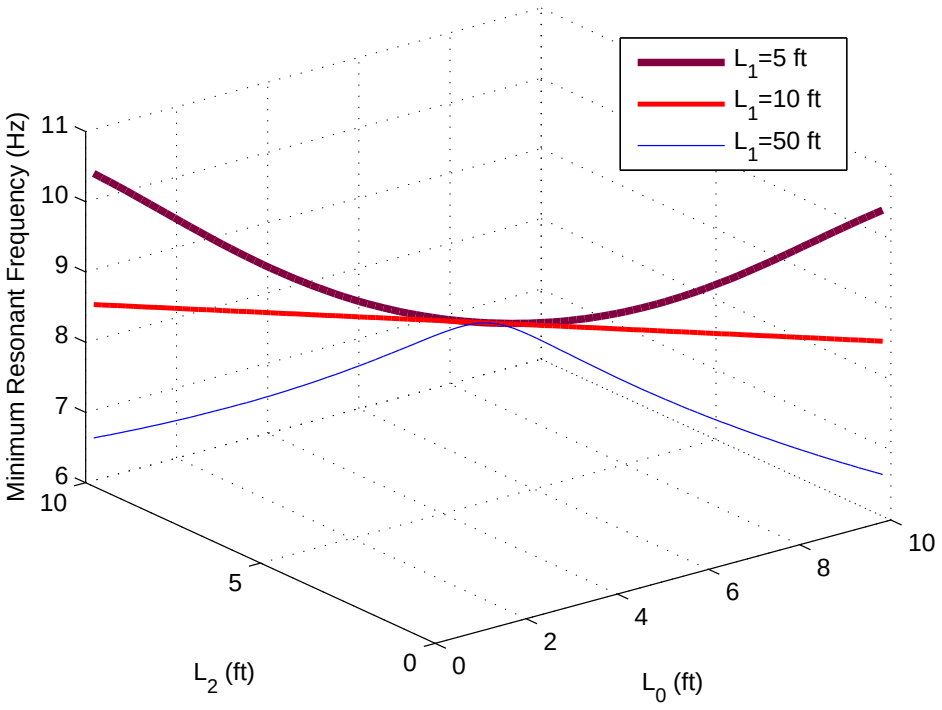

Figure 3.11: Two-idler system minimum resonant frequency: $L_0 + L_2 = 10$ ft

3.4.2 Three-Idler System

Numerical simulations for the three-idler system with a procedure similar to the two-idler case give some useful insights into the behavior of the minimum resonant

frequency. The first observation is related to the symmetric property of the span length distribution which is similar to the one discussed for the two-idler case. If the minimum resonant frequency f_1 is written as a function of all span lengths, $f_1 = f_1(L_0, L_1, L_2, L_3)$, then the following relationship can be obtained:

$$f_1(L_0, L_1, L_2, L_3) = f_1(L_3, L_2, L_1, L_0) \neq f_1(L_0, L_2, L_1, L_3) = f_1(L_3, L_1, L_2, L_0)$$

The procedure followed for the three-idler system: Choose $L_1 = L_2 = 40$ ft, vary the total span length of the first and last span, $L_0 + L_3 = 2L$ from 20 ft to 60 ft in steps of 5 ft, and for each total span length value the same strategy as in the two-idler case is employed. The minimum resonant frequency as a function of L_0 and L_3 is shown in Figure 3.12.

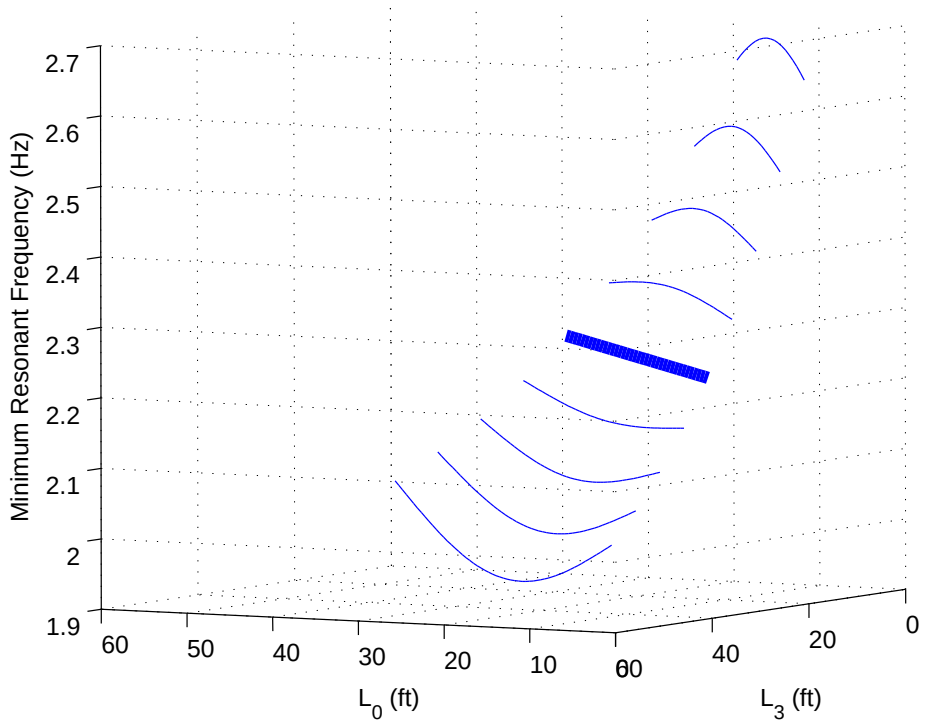

Figure 3.12: Three-idler system minimum resonant frequency: $L_1 = L_2 = 40$ ft, $L_0 + L_3 = 2L$ and $2L = 20$ to 60 ft

In Figure 3.12, the middle thick straight line corresponds to the case when $L_0 +$

$L_3 = L_1 = L_2 = 40$ ft, and the following observations can be drawn:

1. If $L_0 + L_3 = 2L < L_1$, choosing $L_0 = L_3 = L$ will maximize the minimum resonant frequency.

2. If $L_0 + L_3 = L_1 = L_2$, any combination of L_0 and L_3 will result in the same minimum resonant frequency.

3. If $L_0 + L_3 = 2L > L_1$, f_1 is maximized by increasing $|L_0 - L_3|$. The minimum value of f_1 will be attained when $L_0 = L_3 = L$.

3.4.3 Four-Idler System

The following observations about the minimum resonant frequency can be drawn from the numerical simulations for the four-idler system:

1. If $L_0 = L_4$ and $L_1 = L_3$, $f_1(L_0, L_1, L_2, L_3, L_4) = f_1(L_0, L_1, \alpha L_2, L_3, L_4)$ where $\alpha > 0$, that is, the minimum resonant frequency, f_1, is independent of L_2.

2. The symmetry property also applied to the four-idler case, that is, $f_1(L_0, L_1, L_2, L_3, L_4) = f_1(L_4, L_3, L_2, L_1, L_0)$.

The minimum resonant frequency as a function of L_0 and L_4 is shown in Figure 3.13 with the following numbers: $L_1 = L_3 = 30$ ft, $L_2 = 40$ ft, and $L_0 + L_4 = 2L$ varies from 20 ft to 60 ft in steps of 5 ft. In the figure, the middle thick line corresponds to the case $L_0 + L_4 = L_2 = 40$ ft.

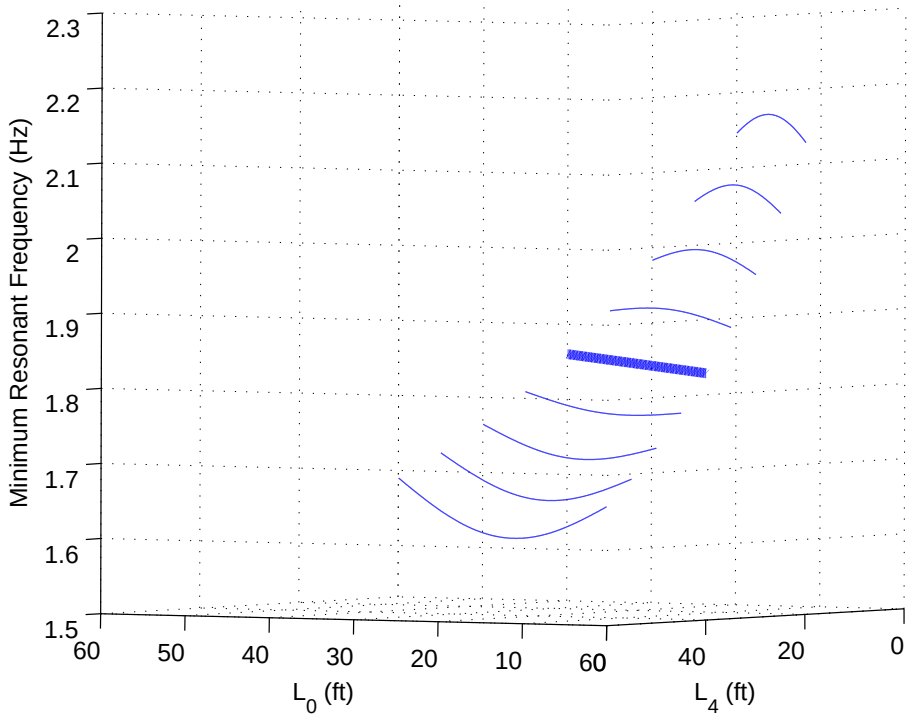

Figure 3.13: Four-idler system minimum resonant frequency: $L_1 = L_3 = 30$ ft, $L_2 = 40$ ft, $L_0 + L_4 = 2L$ and $2L = 20$ to 60 ft

The following additional observations can be made based on the numerical simulations:

1. If $L_0 + L_4 = 2L < L_2$, choosing $L_0 = L_4 = L$ will maximize the minimum resonant frequency.

2. If $L_0 + L_4 = L_2$, any combination of L_0 and L_4 will result in the same minimum resonant frequency.

3. If $L_0 + L_4 = 2L > L_2$, f_1 can be increased by increasing the quantity $|L_0 - L_4|$. The minimum value for f_1 will be attained when $L_0 = L_4 = L$.

In addition, a simulation result similar to Figure 3.11 for the two-idler case is generated for the four-idler case as shown in Figure 3.14.

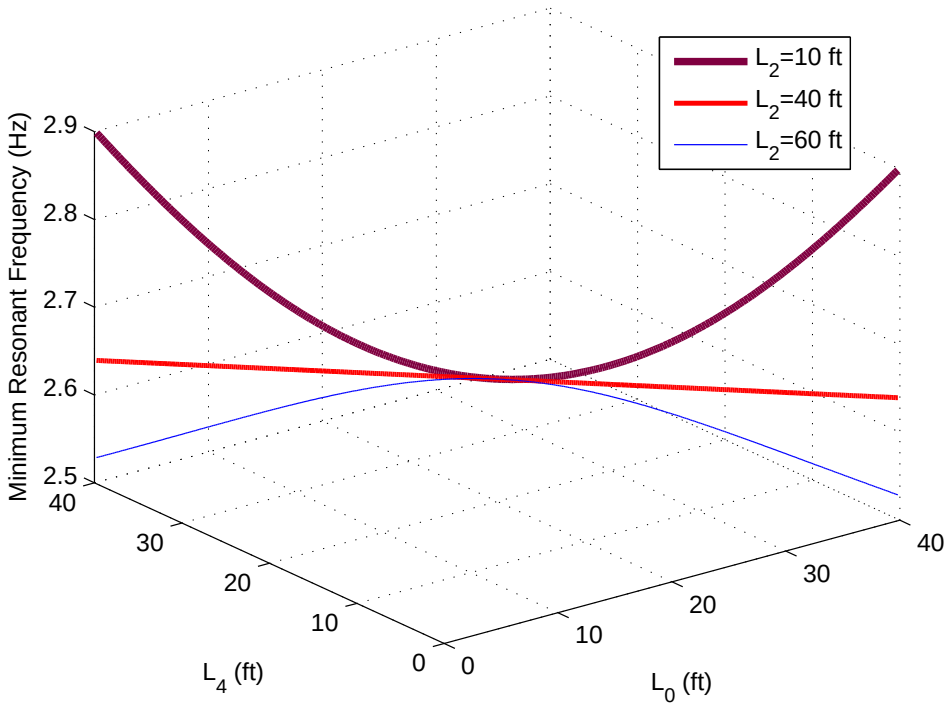

Figure 3.14: Four-idler system minimum resonant frequency: $L_0 + L_4 = 40$ ft, $L_1 = L_3 = 20$ ft and varying L_2

3.4.4 Effect of EA/m

Since the minimum resonant frequency is a function of the quantity $\sqrt{EA/m}$ (as is evident from the expressions for the one- and two-idler cases), it is reasonable to assume that it affects the minimum resonant frequency of the other idler systems in a similar fashion. Numerical simulations have been done to verify this by fixing the total length of all the spans, varying number of idlers, and considering three values for the quantity EA – 1000 lbf, 2000 lbf, and 4000 lbf. Figure 3.15 shows the results of the simulation. It is clear that increasing EA increases the minimum resonant frequency while increasing the number of idle rollers, for the same total length of spans, decreases the minimum resonant frequency.

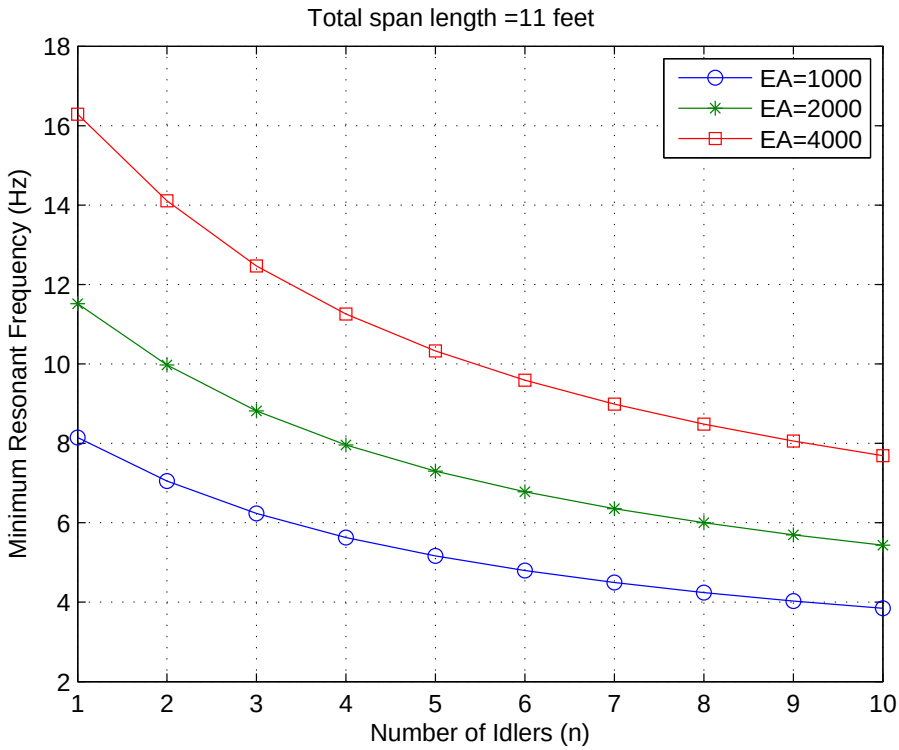

Figure 3.15: Effect of EA on the Minimum Resonant Frequency

3.5 Mass-Spring System Analogy

Based on the considered model for the web span tension dynamics and web velocity on the roller, one can give a mass-spring system analogy for the system of idle rollers and spans. For example, mass-spring systems analogous to the two-idler and four-idler cases are shown in Figures 3.16 and 3.17, respectively. The velocities v_p and v_w are the input web velocities (driven roller velocities are maintained by the control system). Note that the rigid-body mode corresponds to all the involved velocities being equal.

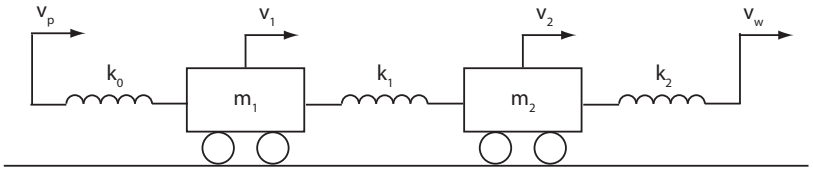

Figure 3.16: Two-Idler System Analogy

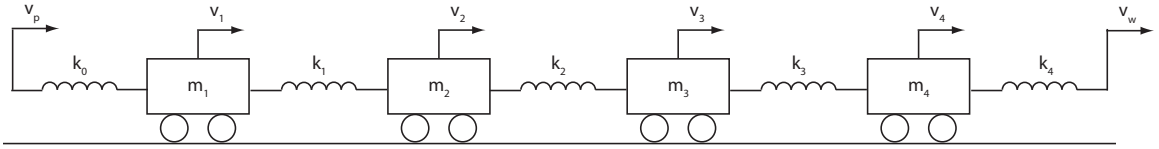

Figure 3.17: Four-Idler System Analogy

The mass-spring system in Figure 3.16 has five independent energy storage elements – 3 springs and 2 masses. Therefore, the motion of the system is characterized by five state variables, these are the forces in the three springs (F_{k0}, F_{k1}, F_{k2}) and the velocities of the two masses (v_1, v_2). The dynamic equations of motion are given by

$$m_1\dot{v}_1 = -F_{k0} + F_{k1}$$

$$m_2\dot{v}_2 = -F_{k1} + F_{k2}$$

$$\dot{F}_{k0} = k_0(v_1 - v_p)$$

$$\dot{F}_{k1} = k_1(v_2 - v_1)$$

$$\dot{F}_{k2} = k_2(v_w - v_2)$$

In matrix form,

$$\begin{bmatrix} \dot{F}_{k0} \\ \dot{v}_1 \\ \dot{F}_{k1} \\ \dot{v}_2 \\ \dot{F}_{k2} \end{bmatrix} = \underbrace{\begin{bmatrix} 0 & k_0 & 0 & 0 & 0 \\ -\frac{1}{m_1} & 0 & \frac{1}{m_1} & 0 & 0 \\ 0 & -k_1 & 0 & k_1 & 0 \\ 0 & 0 & -\frac{1}{m_2} & 0 & \frac{1}{m_2} \\ 0 & 0 & 0 & -k_2 & 0 \end{bmatrix}}_{\mathbf{A}_2} \begin{bmatrix} F_{k0} \\ v_1 \\ F_{k1} \\ v_2 \\ F_{k2} \end{bmatrix} + \begin{bmatrix} -k_0 & 0 \\ 0 & 0 \\ 0 & 0 \\ 0 & 0 \\ 0 & k_2 \end{bmatrix} \begin{bmatrix} v_p \\ v_w \end{bmatrix} \tag{3.34}$$

The equations of motion for the mass-spring system shown in (3.34) are the same as those for two-idler system. Therefore, the forces in the springs are analogous to tensions in the web spans and the velocities of the masses are analogous to web velocities on the rollers.

3.6 Analytical Approximation of the Minimum Resonant Frequency for Equal Span Lengths and Any Number of Idle Rollers

3.6.1 The Approximation Process

An analytical estimate of the minimum resonant frequency of an idler system with any number of equal length spans is derived. One example of such a system is the accumulator system where the span lengths are all equal. The system matrix for an n-idler system is given by

$$\mathbf{A}_n = \begin{bmatrix} 0 & k & & & & \\ -\frac{1}{m} & 0 & \frac{1}{m} & & 0 & \\ & -k & 0 & k & & \\ & & -\frac{1}{m} & 0 & \ddots & \\ & 0 & & \ddots & \ddots & \frac{1}{m} \\ & & & & -k & 0 \end{bmatrix}_{(2n+1)\times(2n+1)} \tag{3.35}$$

where $m = J/R^2$, $k = EA/L$, and L is the web span length.

The eigenvalues of the system matrix $\mathbf{A}_n$ are the roots of the characteristic equa-

tion:

$$\det(sI - \mathbf{A}_n) = \begin{vmatrix} s & -k & & & & \\ \frac{1}{m} & s & -\frac{1}{m} & & 0 & \\ & k & s & -k & & \\ & & \frac{1}{m} & s & \ddots & \\ & 0 & & \ddots & \ddots & -\frac{1}{m} \\ & & & & k & s \end{vmatrix}_{(2n+1)\times(2n+1)} = 0 \tag{3.36}$$

To simplify equation (3.36), the following matrix determinant property will be used: If a row or a column of a determinant is divided by a scalar k, then the determinant is divided by k. Also note that the dimension of the system matrix is always odd, $2n + 1$. With these properties in mind, the characteristic equation can be obtained by the following procedure:

1. Define $s = p\omega$ where $\omega = \sqrt{k/m}$=$\sqrt{EA/mL}$. Substitute this into equation (3.36) to get $\det(p\omega I - \mathbf{A}_n)$.

2. Divide all odd rows and even columns of $\det(p\omega I - \mathbf{A}_n)$ by $\sqrt{k}$.

3. Divide all even rows and odd columns of $\det(p\omega I - A_n)$ by $\sqrt{1/m}$.

4. Define a special determinant as:

$$D_i = \begin{vmatrix} p & -1 & & & & \\ 1 & p & -1 & & 0 & \\ & 1 & p & -1 & & \\ & & 1 & p & \ddots & \\ & 0 & & \ddots & \ddots & -1 \\ & & & & 1 & p \end{vmatrix}_{i\times i}$$

Now,

$$\det(sI - A_n) = \omega^{2n+1} D_{2n+1} = \omega^{2n+1} \begin{vmatrix} p & -1 & & & & \\ 1 & p & -1 & & 0 & \\ & 1 & p & -1 & & \\ & & 1 & p & \ddots & \\ & 0 & & \ddots & \ddots & -1 \\ & & & & 1 & p \end{vmatrix}_{(2n+1)\times(2n+1)} = 0 \tag{3.37}$$

For D_i, the following recursive equation is valid:

$$D_i = pD_{i-1} + D_{i-2} \qquad (i = 3, 4, \cdots) \tag{3.38}$$

One can easily compute $D_1 = p$ and $D_2 = p^2 + 1$; using these two as initial conditions, D_{2n+1} can be obtained by applying equation (3.38) recursively. The roots of $D_{2n+1} = 0$ are obtained first, followed by the resonant frequencies: If p is a root of $D_{2n+1} = 0$, the corresponding resonant frequency is given by

$$f = \frac{|s|}{2\pi} = \frac{|p\omega|}{2\pi} = \left| \frac{1}{2\pi} p \sqrt{\frac{EA}{mL}} \right| \text{ Hz} \tag{3.39}$$

It is possible to obtain a lower bound of the minimum resonant frequency by considering the characteristic polynomial $D_{2n+1} = 0$ which is given by

$$p(p^{2n} + c_{2(n-1)} p^{2(n-1)} + \cdots c_2 p^2 + c_0) = 0 \tag{3.40}$$

The values of c_0 and c_2 for increasing number of idle rollers are given in Table (3.1).

n	c_0	c_2
1	$2 = 1 + 1$	1
2	$3 = 2 + 1$	4
3	$4 = 3 + 1$	$10 = 3^2 + 1^2$
4	$5 = 4 + 1$	$20 = 4^2 + 2^2$
5	$6 = 5 + 1$	$35 = 5^2 + 3^2 + 1^2$
6	$7 = 6 + 1$	$56 = 6^2 + 4^2 + 2^2$
7	$8 = 7 + 1$	$84 = 7^2 + 5^2 + 3^2 + 1^2$
8	$9 = 8 + 1$	$120 = 8^2 + 6^2 + 4^2 + 2^2$

Table 3.1: Values of c_0 and c_1 as a function of n

By induction, the coefficients c_0 and c_2 for the general case of an n-idler system are given by

$$\begin{aligned} c_0 &= n + 1 \\ c_2 &= \sum_{i=0}^{floor(n/2)} (n - 2i)^2 \qquad \text{when } n > 2 \end{aligned} \tag{3.41}$$

where, for odd n, the function $floor(n/2)$ gives the largest integer number smaller than $n/2$.

Define p_{nmin} as the minimum root of $D_{2n+1} = 0$, then the value of p_{2min} can be obtained through a easy computation as $p_{2min} = 1$. Note p_{nmin} is proportional to the minimum natural frequency of an n-idler system which has $(n - 2)$ extra idlers and web spans compared to the two-idler case. Also consider the fact that the larger number of idlers and longer total span length in the system will result in a smaller minimum natural frequency, the following is true:

$$p_{nmin} < p_{2min} = 1 \qquad \text{when } n > 2 \tag{3.42}$$

The higher powers of p_{nmin} would be much smaller when $n > 2$. Hence, the charac-

teristic equation $D_{2n+1} = 0$ can be approximated by

$$p(c_2 p^2 + c_0) = 0 \tag{3.43}$$

Since the complex conjugate roots of the above equation are $\pm j\sqrt{(c_0/c_2)}$, an estimate of the minimum resonant frequency f_1 (in Hz) is given by

$$\hat{f}_1 = \frac{\omega}{2\pi}\sqrt{\frac{c_0}{c_2}} \tag{3.44}$$

In summary, for an n-idler system with identical idlers and equal span lengths, L, an estimate of the minimum resonant frequency is

$$\hat{f}_1 = \frac{\omega}{2\pi}\sqrt{\frac{n+1}{\sum_{i=0}^{(floor(n/2))}(n-2i)^2}} \qquad \text{when } n > 2 \tag{3.45}$$

Further, this estimate is a lower bound on the minimum resonant frequency, so it can be safely used. Table (3.2) gives the values of the estimate and the actual frequency for values of n ranging from 1 to 10. It can be observed that as the number of idlers is increased, the estimate tends to converge to the actual system minimum natural frequency.

Number of Idlers n	Estimated $2\pi\hat{f}_1/\omega$	Actual $2\pi f_1/\omega$
1	1.4142	1.4142
2	0.8660	1.0000
3	0.6325	0.7654
4	0.5000	0.6180
5	0.4140	0.5176
6	0.3536	0.4450
7	0.3086	0.3902
8	0.2739	0.3473
9	0.2462	0.3129
10	0.2236	0.2846

Table 3.2: Estimated and actual minimum resonant frequencies

3.6.2 Minimum Resonant Frequency of an Accumulator System

Accumulators are primarily used to allow stoppage of an unwinder for splicing or a winder for cutoff and changing to a new core, while the whole web processing line continues at a constant velocity. An accumulator system usually has a large number of idlers with equal span lengths between them, which makes it an ideal example to apply the approximation method mentioned above to calculate the system minimum resonant frequency.

Assume a hypothetical accumulator system consisting of nine (9) idler rollers. These idle rollers are all identical with radius R equal to 0.125 ft and inertia J equal to 0.00217 lbf-ft-s^2, that is $m = J/R^2 = 0.1389$ lbf-ft^{-1}-s^2. The span length L (height of the accumulator) between these idlers varies from 15 ft to 1 ft. The web material in the accumulator has an EA value equal to 2000 lbf. The approximate minimum resonant frequency of the accumulator when its moving carriage is at its highest position ($L_H = 15$ ft) is given by:

$$\hat{f}_{1H} = \frac{0.2462\omega}{2\pi}\sqrt{\frac{EA}{mL_H}} = \frac{0.2462}{2\pi}\sqrt{\frac{EA}{15m}} = 1.214 \text{ Hz} \tag{3.46}$$

While, when the carriage is at its lowest position ($L_L = 1$ ft), the minimum resonant frequency is:

$$\hat{f}_{1L} = \frac{0.2462\omega}{2\pi}\sqrt{\frac{EA}{mL_L}} = \frac{0.2462}{2\pi}\sqrt{\frac{EA}{1m}} = 4.7 \text{ Hz} \tag{3.47}$$

These calculations can assist in the design of number of accumulator spans and the maximum travel of the accumulator carriage.

3.7 Summary and Conclusions

The resonant frequencies of an idler system are usually ignored during web handling system modeling and controller design phases. To demonstrate the importance of the resonant frequencies, a simple frequency response experiment was conducted. A velocity disturbance was injected simultaneously into the 5-idler pull roll section

system (Figure 3.5) and 5-idler rewind section system (Figure 3.3) of the EWL. The amplitude of the disturbance M was set to be 10 FPM, and the disturbance frequency ν changed from 5.6 Hz to 6.2 Hz. Note 5.6 Hz is the minimum resonant frequency of the idler system in the pull roll section, and 6.2 Hz is the minimum resonant frequency of the idler system in the rewind section. The tension responses from both of these two systems are shown in Figure 3.18. It is evident that different idler systems have different tension responses to the same velocity disturbance, and the web tension variation will become more severe as the disturbance frequency is close to the system resonant frequency.

A simple dynamic model for web tension dynamics within a span is considered for predicting the resonant frequencies in a subsection of a web line between two driven rollers containing idle rollers and spans. Based on this model, one can write the system dynamics for any number of idle rollers and spans, and the system matrix is a tridiagonal matrix which is suitable for analytical and numerical analysis. The ability of the model to predict resonant frequencies (at least the minimum resonant frequency) was verified by conducting experiments on a web line, and comparing the data from experiments and model simulations.

Analytical expressions of the resonant frequencies for the one- and two-idler systems are given and discussed. The focus of this is on the effect of span lengths on the resonant frequency; it was assumed that the idle rollers are identical for both analytical and numerical analysis. In the one-idler case, it may be seen that the minimum value of the resonant frequency occurs when the span lengths adjacent to the idle roller are equal. For the two-idler case, two useful observations can be made: (1) If the length of the two end spans are equal, then the minimum resonant frequency does not depend on the middle span length. (2) The two end span lengths can be interchanged without affecting the resonant frequencies. Numerical analysis was also done for the three- and four-idler cases. It was found that behavior of the

minimum resonant frequency is symmetric in terms of span lengths similar to that of the two-idler case.

For systems containing identical rollers with equal span lengths (such as an accumulator), an estimate of the minimum resonant frequency is provided in terms of the number of idle rollers. The estimate is a lower bound on the minimum resonant frequency, and approaches the actual value with an increase in the number of idle rollers.

This study is expected to assist the web machine designer as well as the control systems engineer. For the web machine designer, it helps in the selection of span lengths and placement of idle rollers to maximize the minimum resonant frequency, and in designing the machine structure to avoid web and idle roller induced resonances. For the control system engineer, this leads to limitations on the bandwidth of the overall closed-loop system, that is, one has to select the control system bandwidth to be less than the system's minimum resonant frequency.

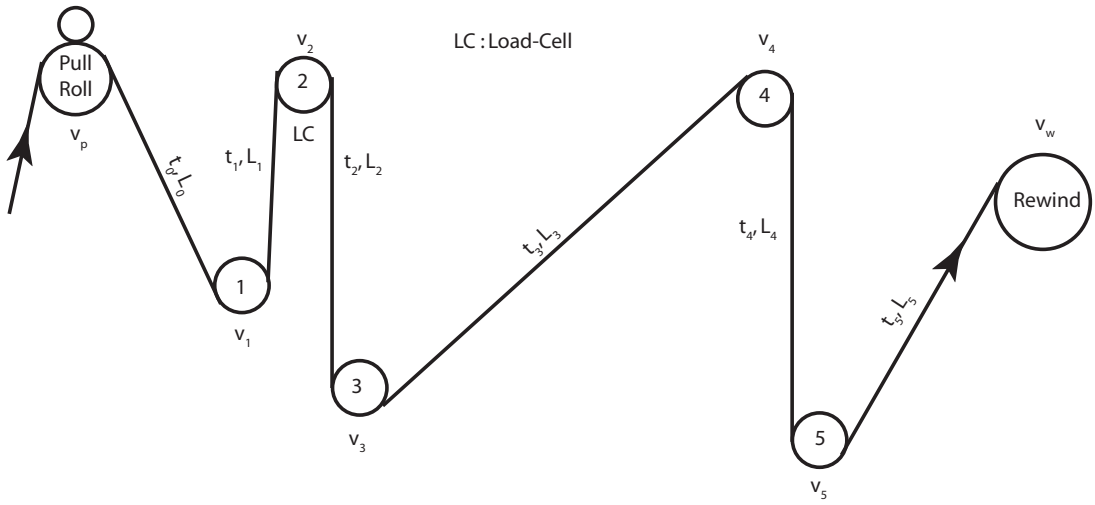

L_0	L_1	L_2	L_3	L_4	L_5
32.5”	19.8”	31.2”	54.5”	34.8”	32.6”

Figure 3.3: Rewind Section: Five-Idler System Configuration

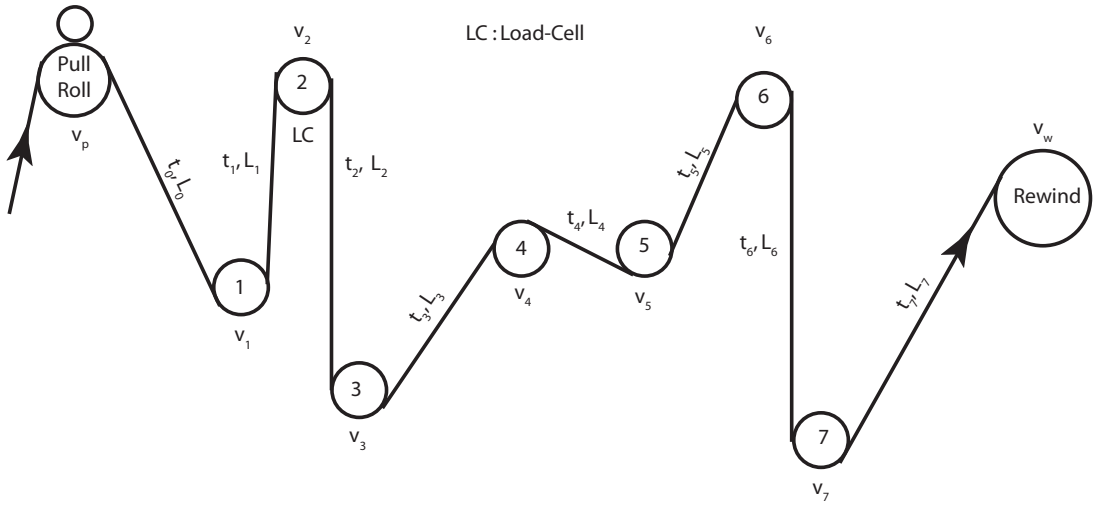

L_0	L_1	L_2	L_3	L_4	L_5	L_6	L_7
32.5”	19.8”	31.2”	26.8”	5.3”	23.3”	34.8”	32.6”

Figure 3.4: Rewind Section: Seven-Idler System Configuration

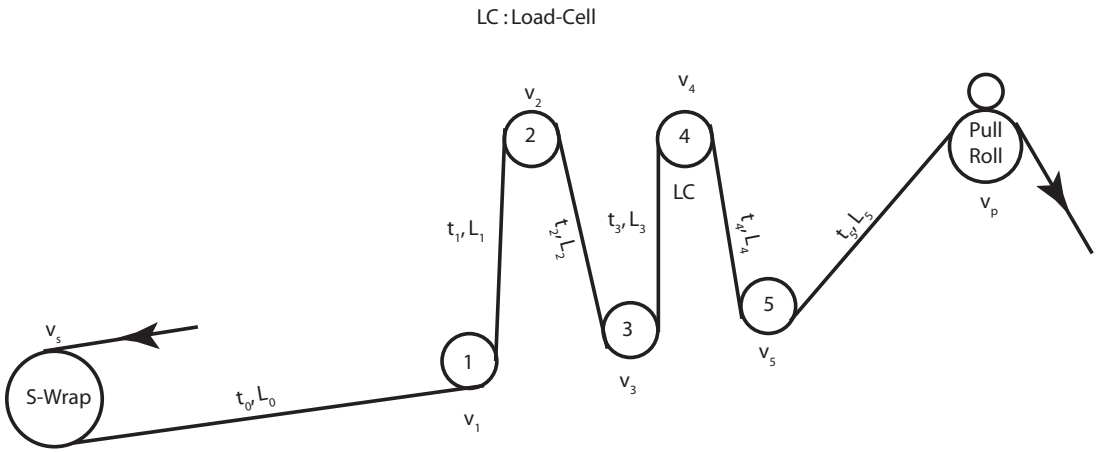

L_0	L_1	L_2	L_3	L_4	L_5
65.3”	34.2”	13.0”	14.3”	16.0”	35.0”

Figure 3.5: Pull Roll Section: Five-Idler System Configuration

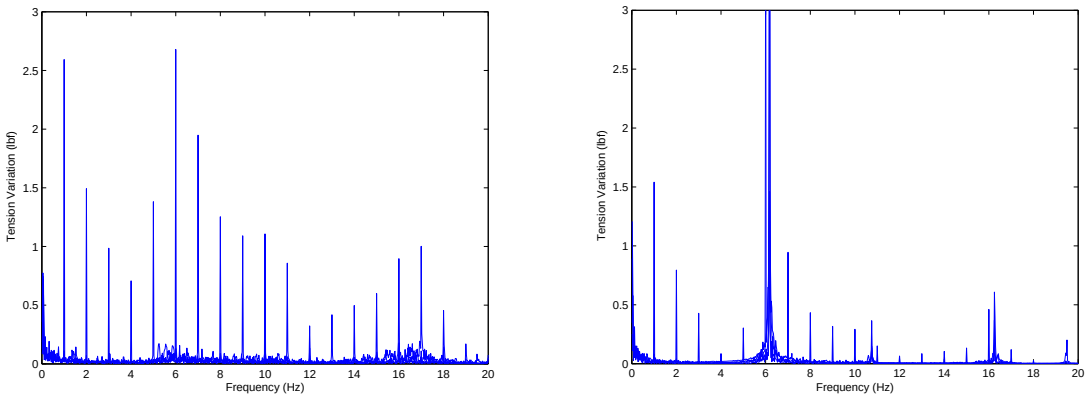

(a) Experiment Data

(b) Model Simulation Result

Figure 3.6: Rewind Section: Five-Idler System Frequency Response Comparison

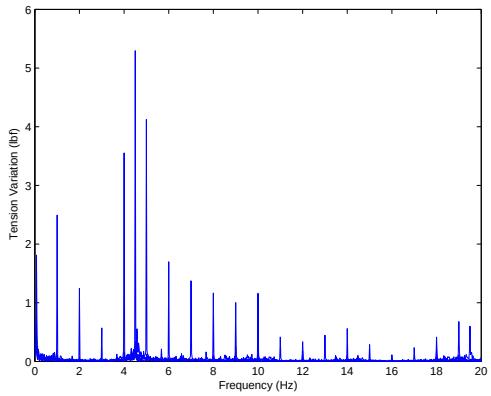

(a) Experiment Data

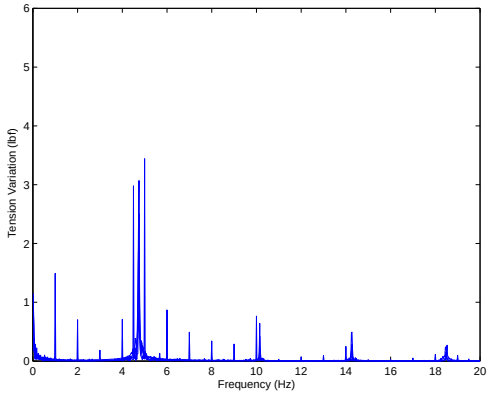

(b) Model Simulation Result

Figure 3.7: Rewind Section: Seven-Idler System Frequency Response Comparison

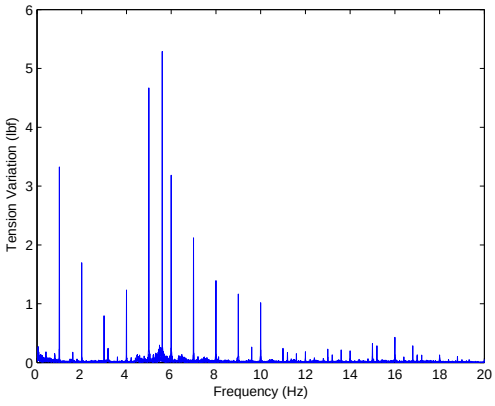

(a) Experiment Data

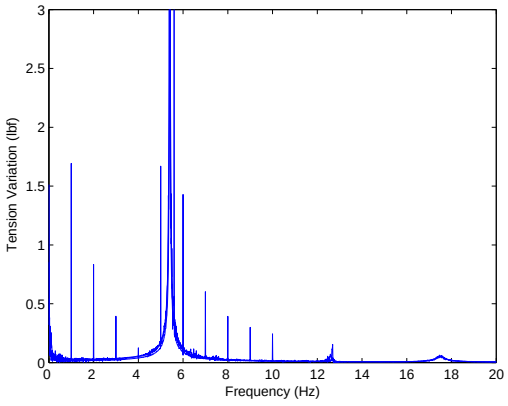

(b) Model Simulation Result

Figure 3.8: Pull Roll Section: Five-Idler System Frequency Response Comparison

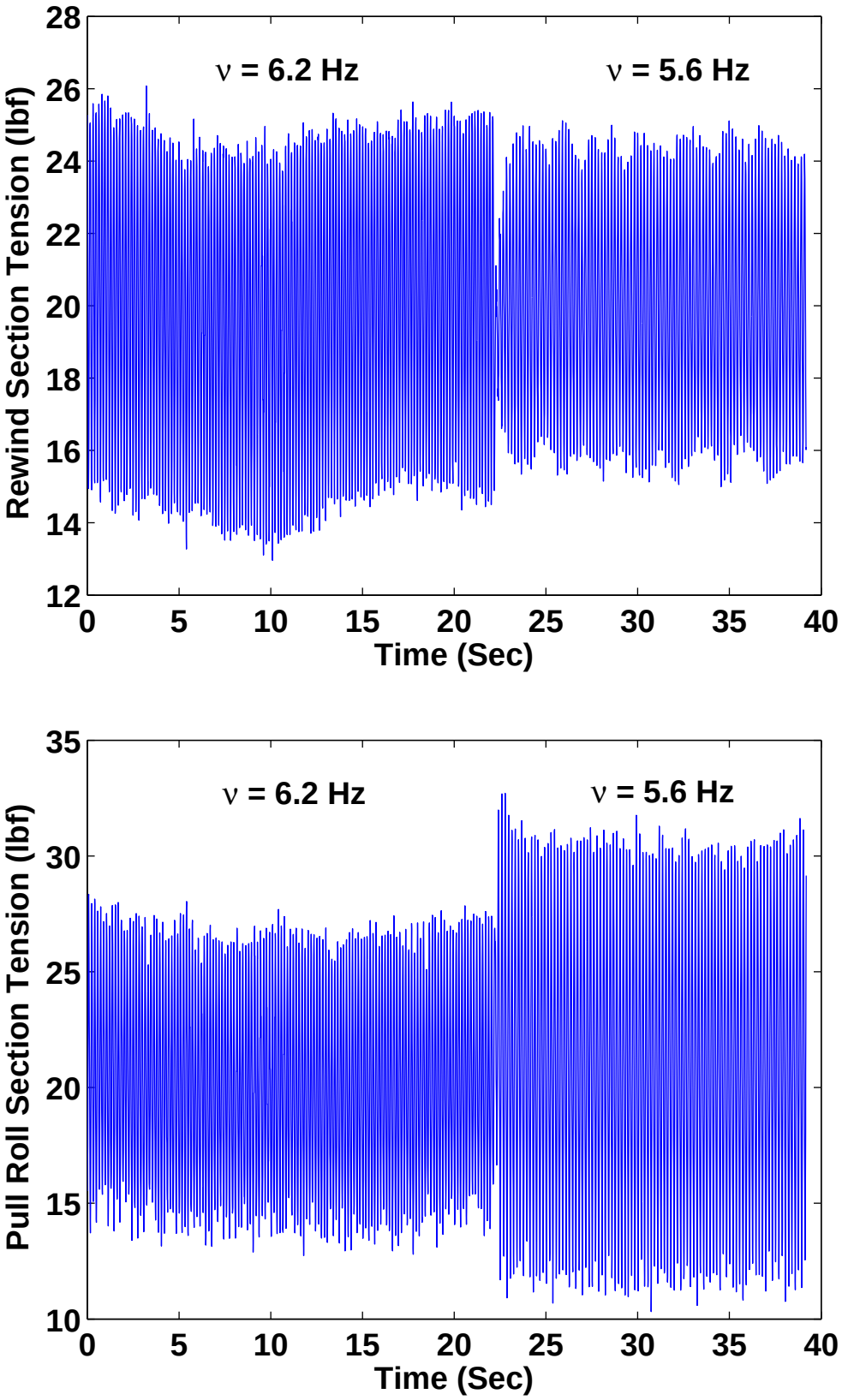

Figure 3.18: Pull Roll and Rewind Section Tension Response Comparison

CHAPTER 4

DESIGN AND IMPLEMENTATION OF A KALMAN FILTER FOR WEB TENSION

4.1 Introduction

Web tension and velocity are two key variables that influence the quality of the finished web and hence the products manufactured from it. It is extremely important in web process lines to maintain proper web tension in different tension zones while accurately controlling web transport velocity. In a feedback control system, the quality of the feedback signal has a vital impact on the final control performance. For a web handling system, two most important feedback signals that need to be measured are web velocity and tension. The velocity of the web line can usually be measured by an encoder installed on the shaft of a roller, and the encoder can provide a relatively precise and noise-free velocity feedback since the encoder basically only contains digital circuits, but this is not true for the web tension measurement.

The web tensions are usually measured by load cell sensors installed on the idle rollers of the web line. A load cell is classified as a force transducer. This device converts force or weight into an electrical signal. The heart of the load cell is the strain gage(s) which is a device that changes resistance when it is stressed. In a loadcell, multiple strain gages are connected to create the four legs of a Wheatstone-bridge configuration. When an input voltage is applied to the bridge, the output becomes a voltage proportional to the force on the cell. This output then will be amplified and processed by a signal conditioner to form a standard analog signal. Figure 4.1 shows a load cell roller in the EWL. The tension signal conditioner and display unit

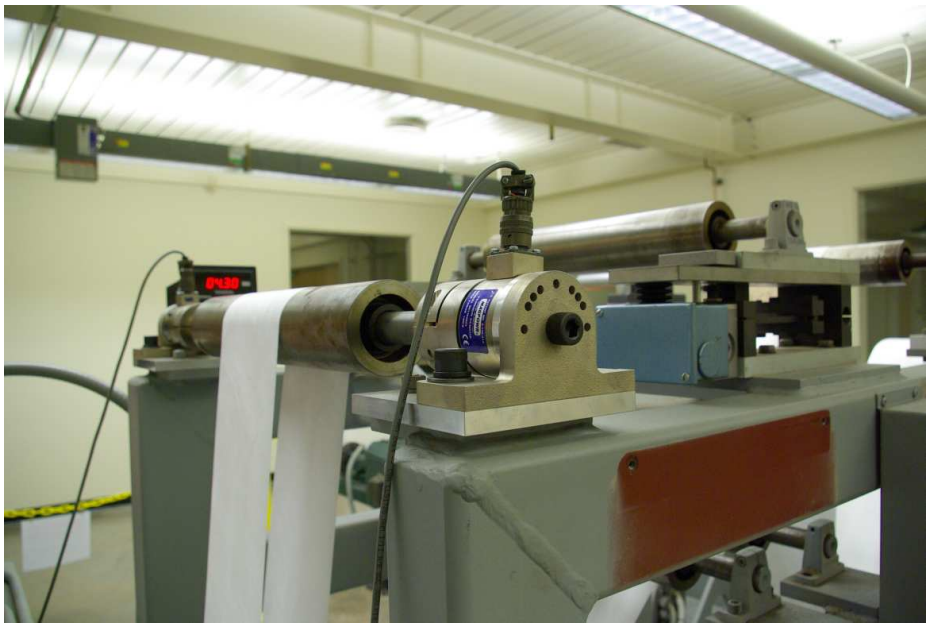

Figure 4.1: Load Cell Roller in EWL

Figure 4.2: Tension Signal Conditioner and Display Unit in EWL

is shown in Figure 4.2. The load cell systems in EWL have a measurement range of 0 to 50 lbf of web tension, which is converted to a $0-10$ V analog voltage output [18]. Due to its working principle, the load cell system which includes the load cells, the cable and the signal conditioner is an analog signal process circuit. The tension feedback signal, the output of the analog circuit, can be easily contaminated by the noise components from the strain gages, the signal conditioner and the environment.

In order to overcome this problem and provide an optimal web tension estimation to the controller in the presence of noise, a tension signal Kalman filter was designed and implemented in the tension control system feedback loop, and experiments were conducted to demonstrate the effect of the filter on the tension feedback signal.

4.2 Kalman Filter Design

4.2.1 General System Model

A practical linear discrete system with noise may be described by [12]:

$$x(k+1) = Ax(k) + Bu(k) + Gw(k) \tag{4.1}$$

$$y(k) = Cx(k) + v(k) \tag{4.2}$$

with state $x(k) \in \mathbb{R}^n$, control input $u(k) \in \mathbb{R}^m$ and measured output $y(k) \in \mathbb{R}^p$. The process noise $w(k)$ represents disturbances or modeling inaccuracies of the system such as uncertainties during modeling process and plant parameter variations; the measurement noise $v(k)$ is the sensing inaccuracy due to the existence of noise. It is assumed that $w(k)$ is a stationary white noise process with zero mean and known covariance of $Q \geqslant 0$ written as $w(k) \sim (0, Q)$. It is also assumed that $v(k) \sim (0, R)$ where $R > 0$.

Assume that w_k and v_k are mutually uncorrelated so that $\mathrm{E}\left\{w_j v_k^T\right\} = 0$ for all j and k. That is, the process and measurement noises arise in the system from independent effects, which makes sense practically. The initial state x_0 is also unknown, but

we do have some knowledge of x_0 in the form of its mean value $\hat{x}_0$ and covariance P_0, thus, $x_0 \sim (\hat{x}_0, P_0)$. Finally, as covariance matrices, P_0, Q and R are also symmetric.

4.2.2 The Discrete Recursive Kalman Filter

The Kalman filter aims to provide an optimal estimated internal state $\hat{x}_k$ by only using information from the previous step and current step as well as considering the existence of noise. Since it is easy to implement, requires small storage memory space and relatively low computation load, the Kalman filter method has been widely used in autopilot, computer vision and robotic areas. A brief discussion of the discrete recursive Kalman filter is given below.

Let the estimate at time k before the measurement y_k is taken be denoted by $\hat{x}_k^-$. This is called the a priori estimate. Define the a priori error covariance P^- at time k as:

$$P_k^- = \mathrm{E}\left\{\left(x_k - \hat{x}_k^-\right)\left(x_k - \hat{x}_k^-\right)^T\right\} \tag{4.3}$$

Then a discrete-time recursive Kalman filter can be expressed by the following equations:

- Kalman gain:

$$K_k = P_k^- C^T \left(CP_k^- C^T + R\right)^{-1} \tag{4.4}$$

- Estimate Recursion:

$$\hat{x}_{k+1}^- = A\hat{x}_k^- + Bu_k + AK_k\left(y_k - C\hat{x}_k^-\right) \tag{4.5}$$

- Error Covariance Recursion:

$$P_{k+1}^- = A\left[P_k^- - P_k^- C^T \left(CP_k^- C^T + R\right)^{-1} CP_k^-\right] A^T + GQG^T \tag{4.6}$$

The estimate recursion equation (4.5) is of the same form as a deterministic Luenberger observer but with a time-varying gain AK_k, and the Kalman gain equation

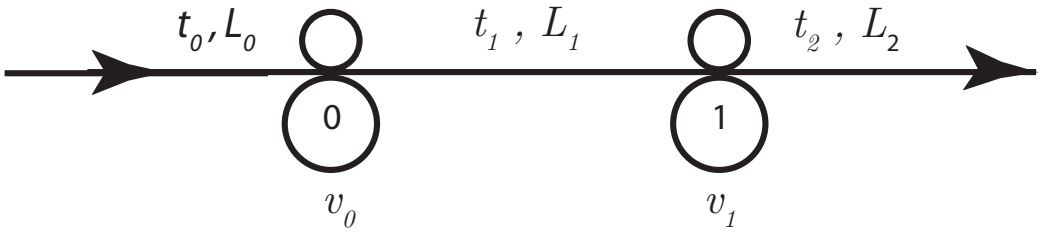

Figure 4.3: A Web Span Between Two Driven Rollers

(4.6) is the discrete time Riccati equation for P_k^-. As long as the filter is initialized, that is to assign initial values for P_0^- and $\hat{x}_0^-$, it can continuously provide an optimal estimate of the system state $\hat{x}^-$ to minimize the system error covariance P^-.

4.2.3 Web Span Tension System Model

For a web span between two driven rollers shown in Figure 4.3, recalling the detailed derivation in section 3.2.1 and referring to (3.13), the nonlinear dynamic equation of web tension is given by

$$L_1\dot{t_1} = EA\,[v_1 - v_0] + t_0 v_0 - t_1 v_1 \tag{4.7}$$

where t_1 is the web span tension, t_0 is the web tension in the previous web span, L_1 is the span length, E is the tensile modulus of elasticity of the web in the longitudinal direction, A is the area of cross-section of the web, and v_0 and v_1 are the line speed of the two driven rollers.

Define the following variables: $T_i = t_i - t_{ri}$ and $V_i = v_i - v_{ri}$, where t_{ri} and v_{ri} are tension and velocity references for the $i-$th span and driven roller, respectively, T_i and V_i are the variations in tension and velocity around their reference values. Then, the web tension dynamics (4.7) can be written as

$$L_1\dot{T}_1 = EA\,[(V_1 + v_{r1}) - (V_0 - v_{r0})] + (T_0 + t_{r0})(V_0 + v_{r0}) - (T_1 + t_{r1})(V_1 + v_{r1}) \tag{4.8}$$

In (4.8), assuming $\dot{T}_1$, T_1, T_0, V_1, V_0 to be zero at the forced equilibrium, the

relationship between the system's reference velocities is given by

$$v_{r0} = \frac{AE - t_{r1}}{AE - t_{r0}} v_{r1} \tag{4.9}$$

Substituting (4.9) into (4.8), the error dynamics of the web tension system [5] can be written as

$$L_1 \dot{T}_1 = EA\left[V_1 - V_0\right] + T_0 v_{r0} + t_{r0} V_0 + T_0 V_0 - T_1 v_{r1} - t_{r1} V_1 - T_1 V_1 \tag{4.10}$$

The following assumptions are made in order to simplify the nonlinear equation (4.10):

- The products of variations, $T_i V_i$, are negligible.
- The pull roll is running exactly at the reference velocity, that is $V_0 = 0$.
- The tension reference $t_{r0} = t_{r1} = t_r$, which implies $v_{r0} = v_{r1} = v_r$ according to (4.9).
- The web tension of the previous span, t_0, is regulated well, that is $t_0 = t_r$ and $T_0 = 0$.

Then the nonlinear error dynamics (4.10) can be simplified to a linear single input single output (SISO) system equation

$$L_1 \dot{T}_1 = EAV_1 - T_1 v_r - t_r V_1 \tag{4.11}$$

And the transfer function between web tension variation T_1 and velocity difference of two driven rollers V_1 can be derived from (4.11)

$$G_T(s) = \frac{T_1(s)}{V_1(s)} = \frac{EA - t_r}{L_1 s + v_r} \tag{4.12}$$

4.2.4 Kalman Filter Equations for Web Tension System

Equation (4.12) should be discretized in order to apply the proposed Kalman filter. Applying a ZOH and discretizing the transfer function, the discrete-time tension error

dynamics can be written as:

$$T_1(k+1) = e^{-bT_s}T_1(k) + \frac{a}{b}(1-e^{-bT_s})V_1(k) \tag{4.13}$$

$$y(k) = T_1(k) \tag{4.14}$$

where $a = (EA - t_r)/L_1$, $b = v_r/L_1$ and T_s is the sampling time. Compare (4.13), (4.14) with (4.1), (4.2), the following are the system parameters:

$$\begin{aligned} A &= e^{-bT_s} \\ B &= \frac{a}{b}(1-e^{-bT_s}) \\ G &= 1 \\ C &= 1 \end{aligned} \tag{4.15}$$

Notice these parameters are all scalars, substituting them into Kalman filter equations (4.4), (4.5), and (4.6), the Kalman filter for web tension system can be written as

$$K_k = \frac{P_k^-}{P_k^- + R} \tag{4.16}$$

$$\begin{aligned} \hat{T}_1^-(k+1) &= e^{-bT_s}\hat{T}_1^-(k) + \frac{a}{b}(1-e^{-bT_s})V_1(k) \\ &\quad + e^{-bT_s}K_k\left(T_1(k) - \hat{T}_1^-(k)\right) \end{aligned} \tag{4.17}$$

$$P_{k+1}^- = \left(e^{-bT_s}\right)^2\left(\frac{1}{P_k^-} + \frac{1}{R}\right)^{-1} + Q \tag{4.18}$$

Notice that the Kalman gain K_k is time-varying and dependent on P_{k+1}^-, the solution of the discrete time Riccati equation (4.18).

4.2.5 The Low-pass Filter property of Kalman Filter

The noise rejection and signal smoothing properties of the Kalman filter are preliminarily investigated using the web tension Kalman filter developed in (4.2.4). In (4.17), by treating the estimated tension $\hat{T}_1^-$ as the system output, the measured tension T_1

as the input and choosing the roller velocity variation $V_1 = 0$, the transfer function from the measurement T_1 to the estimate $\hat{T}_1^-$ can be written as:

$$\frac{\hat{T}_1^-(k)}{T_1(k)} = \frac{e^{-bT_s}K_k}{z - e^{-bT_s}(1 - K_k)} = \frac{AK_k}{z - A(1 - K_k)} \tag{4.19}$$

Since the transfer function (4.19) has a relative degree of one, it shows that the Kalman filter is a low-pass filter with time-varying gain K_k and possesses both noise rejection and signal smoothing properties.

4.3 Euclid Web Line Control Strategy

A detailed description of the control strategy of the driven rolls in the EWL will be given in this section. The five driven rolls can be divided into two groups. The pull roll, S-wrap lead and follower rolls are only used to set up the master speed of the web line, thus they all only have one velocity control loop in order to track the speed reference. The unwind and rewind rolls are also in charge of regulating the web tension in unwind and rewind tension zones. Thus, a cascading control structure is adapted to regulate the web tension and track the line speed reference, and a control gain schedule mechanism is used to compensate the inertia and radius changes in the material rolls. In the following, the method for tension control, taking rewind roll for example, will be discussed first. The control structure for the master speed rolls, taking pull roll for example, will be shown later.

4.3.1 Tension Control Structure in Unwind/Rewind Sections

The control method of the rewind roll will be discussed in detail as an example, since both the unwind and rewind rolls have the same control structure.

The rewind roll uses a cascading tension control strategy shown in Figure 4.4. The inner loop is the velocity loop, and the outer loop is the tension regulation loop. The output of the outer tension loop serves as a reference velocity error correction for the

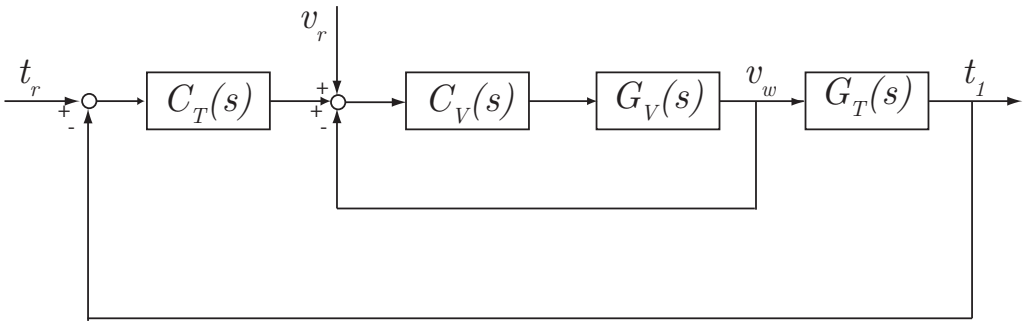

Figure 4.4: Rewind Tension Control Strategy

velocity loop, and the output of the velocity controller $C_V(s)$ is the motor torque. In this control structure, the velocity feedback v_w is provided by an encoder installed on the shaft of the rewind motor, and the web tension feedback t_1 is measured by load cells installed on an idle roller between the pull roll and rewind.

The rewind roll is modeled as an integrator

$$G_V(s) = \frac{1}{J_w s} \tag{4.20}$$

where J_w is the rewind roll total inertia reflected to the motor side.

The tension and velocity controllers $C_T(S)$ and $C_V(S)$ are usually PI controllers. In the EWL, the rewind tension controller $C_T(s)$ is chosen as

$$C_T(s) = \frac{3(s+10)}{s}$$

while the inner velocity PI controller $C_V(s)$ can be expressed as

$$C_V(s) = \frac{k_{ps}(s+\omega_{ld})}{s} \tag{4.21}$$

$$k_{ps} = J_w k_{rf} \tag{4.22}$$

$$\omega_{ld} = k_{rf}/4\zeta^2 \tag{4.23}$$

where k_{rf} , ζ are all design parameters, and the transfer function for the closed inner velocity loop is

$$G_V^{clp}(s) = \frac{C_v(s)G_v(s)}{1+C_v(s)G_v(s)} = \frac{k_{rf}(s+\omega_{ld})}{s^2+k_{rf}s+k_{rf}\omega_{ld}} = \frac{k_{rf}(s+\omega_{ld})}{s^2+2\zeta(2\zeta\omega_{ld})s+(2\zeta\omega_{ld})^2} \tag{4.24}$$

Comparing (4.24) with the standard second order system, it is clear that ζ is the damping ratio of the velocity loop and k_{rf} determines the bandwidth of the system.

The bandwidth and damping of the speed loop should be maintained the same when the web line is running, and since the rewind roll total inertia J_w is time-varying, the values of k_{ps} and ω_{ld} should also be changed accordingly. In order to do so, the controller calculates the winder radius and inertia J_w online periodically and implements a gain schedule on k_{ps} and ω_{ld} according to equations (4.22) and (4.23). A detailed discussion and comparison of different tension control strategies can be found in [19], and it shows that the cascading control scheme can improve the system natural frequency and damping ratio. By applying this gain scheduling on the velocity PI controller, the input step and load response of web tension as well as speed tracking response are improved. On the other hand, due to the physical limitations, such as the maximum torque the driven motor can provide, and stability considerations, the desired bandwidth cannot be always attainable. If the PI gain limits are reached and the system inertia J_w is still increasing, then scheduling of speed loop gains cannot be applied any more; otherwise, the motor torque saturation or system oscillation will occur. The speed loop deterioration in this manner will adversely affect the outer tension loop, thus the application of the cascading control strategy will be restricted when the winder roll system has a large system inertia. In the following experiments, set $k_{rf} = 15$ and $\zeta = 1.1$.

The tension error dynamics $G_T(s)$ in (4.12) is written again here as

$$G_T(s) = \frac{T_1(s)}{V_1(s)} = \frac{EA - t_r}{L_1 s + v_r}$$

where $EA = 2000$ lbf, $L_1 = 17.1$ feet, web velocity reference $v_r = 150$ FPM and the tension reference $t_r = 20$ lbf.

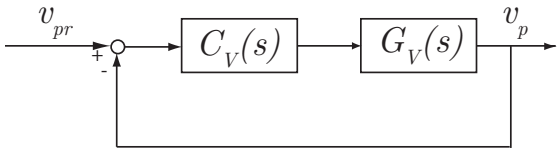

Figure 4.5: Pull roll Velocity Control Strategy

4.3.2 S-wrap and Pull Roll Control Structure

The master speed rolls include the S-wrap lead, follower and pull roll. The control scheme of the pull roll will be discussed here as an example, since all of these master speed rolls share the same control structure.

The pull roll adapts a single velocity control loop as shown in Figure 4.5 where v_{pr} is the pull roll velocity reference and v_p is the actual pull roll velocity. The v_p is measured by an encoder and fed back to the controller $C_V(s)$. The velocity PI controller $C_V(s)$ uses the same control algorithm as described in (4.3.1). For the pull roll, since the roller inertia J_p is a constant, the PI gains are all constants and can be tuned according to (4.22) and (4.23). In the following experiments, for the pull roll PI controller, set $k_{rf} = 40$ and $\zeta = 1.1$.

4.3.3 The Tension Control Scheme With Kalman Filter

Figure 4.6 shows the scheme of the tension error regulation system when the proposed Kalman filter is incorporated. First, the reference tension T_r for the error regulation system is set to be zero such that at the steady state $t_1 = t_r + T_1 = t_r + T_r = t_r$. Second, the inner velocity loop and the tension controller $C_T(s)$ in the feedforward path could be simplified to one single controller $C_{TV}(s)$ as shown in Figure 4.6. The output of $C_{TV}(s)$ is the rewind velocity variation $V_1 = v_w - v_r$. At last, define $T_N = T_1 + N$ as the tension feedback signal with noise, where $T_1 = t_1 - t_r$ is the actual web tension variation and N stands for the noise from the load cells and environmental interference. Due to the existence of the noise N, the controller $C_{TV}(s)$ will actually

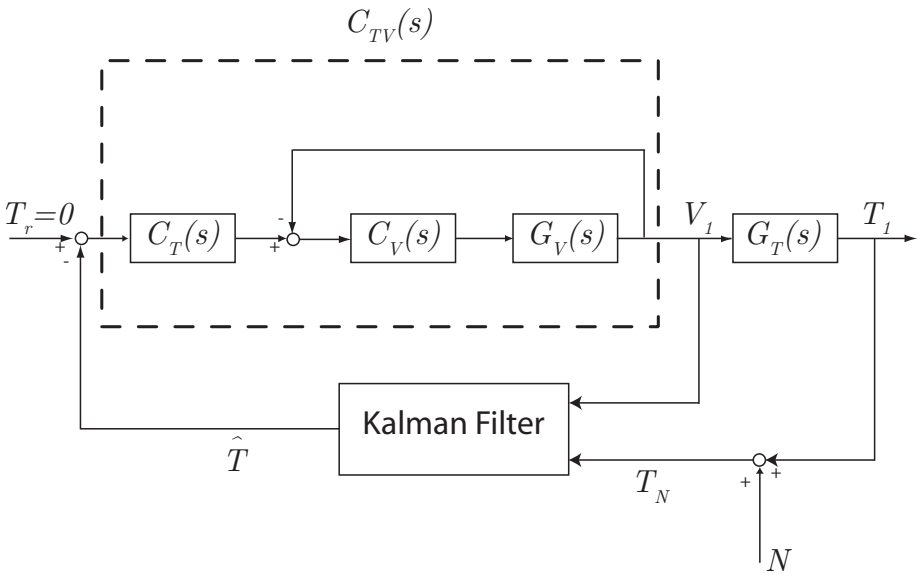

Figure 4.6: Tension Control Scheme with Kalman Filter

deteriorate the web tension regulation quality when the noised tension signal T_N is directly fed back to the controller.

In order to improve tension control quality, a tension Kalman filter as discussed in (4.2.4) is implemented in the feedback path. The Kalman filter takes the noised tension measurement T_N and the control action V_1 as inputs and provides an optimal estimation $\hat{T}$ to the controller.

When investigating the effect of the Kalman filter, a controllable tension signal noise N is desired, thus the Kalman filter can be tested under different noise levels by changing the amplitude of the noise signal. In order to do so, a random number generator based on the Linear Congruential Generator (LCG) method is developed for implementation in the Rockwell ControlLogix system. The generator can produce a pseudo random number series $R(k)$ which has a uniform distribution between -1 and 1. Let $N(k) = MR(k)$ where M is the amplification coefficient, then $N(k)$ is a pseudo random noise signal with a uniform distribution between $-M$ and M.

Referring to tension Kalman filter equations (4.16), (4.17) and (4.18), the parameters and initial values of the Kalman filter in experiments are:

$$Q = 0.2$$

$$R = 8$$

$$P_0^- = 10$$

$$\hat{x}_0^- = T_1$$

$$T_s = 0.01$$

A Kalman filter subroutine was then written accordingly in structure text programming language in RSLogix 5000 software. This subroutine is part of the rewind tension regulation program under the ACDrive controller's 10 ms periodic task. Since all the related computations only involve scalars, the total execution time of the Kalman filter subroutine is estimated to be less than 2 ms, which makes it suitable to be realized in the real-time tension control application.

4.4 Experiments and Results

A series of experiments have been conducted in order to verify the effect of the Kalman filter. The tension regulation performances with and without the Kalman filter are compared in time domain. In order to do so, the standard deviation of the tension signal T_N and T_1 are chosen as indexes. The standard deviation of T_N indicates the noise level of the tension feedback signal, meanwhile, the standard deviation of T_1 shows the system's tension control quality in the web line, that is to say a larger standard deviation of T_1 means that web tension has a larger variation; on the other hand, the smaller T_1 standard deviation stands for a better tension regulation performance.

4.4.1 Experiment Procedure

In the experiments, the tension signal T_1 directly measured by the load cell is regarded as the actual web tension. Then T_1 is summed with the noise signal N to form the simulated noised tension feedback T_N. Finally, the T_1 and T_N are recorded in both of the situations where the proposed Kalman filter is applied and bypassed. The following is the experiment process:

1. Run the web line at the speed of $v_r = 150$ FPM and wait until web tension is regulated around the tension reference $t_r = 20$ lbf.

2. Inject the external noise N and begin to record the web tension T_1 as well as noised tension signal T_N.

3. Keep the noise on, apply the Kalman filter and record T_1, T_N.

4. Process the collected data to get the tension standard deviations of T_1 and T_N in step 2 and 3.

Repeat this process 3 times with the noise amplification coefficient M equal to 2, 5 and 8 lbf separately.

4.4.2 Experimental Results

The experimental results are summarized in Table (4.1). From the table, it is easy to see that the standard deviations of T_1 have been significantly reduced in all three noise level situations after the Kalman filter is applied, which shows the proposed Kalman filter's effect on improving tension control quality in the presence of feedback loop noise N.

Furthermore, the plots of the T_1 before and after the Kalman filter applied with $M = 5$ and $M = 2$ are shown in Figure 4.7 and Figure 4.8 to give visualized testimonies of the Kalman filter's effect. From these figures, it can be seen clearly that

Web Tension Standard Deviation (lbf)		
	Kalman Filter Status	T_1
$M = 2$ lbf	Off	0.438964235
	On	0.303570084
$M = 5$ lbf	Off	0.77761654
	On	0.40137655
$M = 8$ lbf	Off	1.115375427
	On	0.556659829

Table 4.1: The Effect of Kalman Filter on Web Tension Control Quality

the major part of the high frequency components introduced by the noise N have been filtered out by the tension Kalman filter, and the variation amplitude of web tension has also been reduced. Finally, since T_1 is tension variation around reference t_r, it has a zero mean value.

4.5 Summary

In this chapter, a Kalman filter aimed to improve the web tension control quality has been developed and implemented. The general discrete stochastic system model has been introduced. Based on this, a recursive Kalman filter which is easy to implement in real-time control application has been proposed. A simplified web tension error transfer function $G_T(s)$ has been developed from the nonlinear tension dynamic model in (4.7). The linear tension error model is then discretized and a tension Kalman filter is designed based on this model.

The control structures for the master speed rollers and the material rolls in EWL are shown, the cascading tension control strategy and the tuning method for the velocity PI controller are studied. This control strategy and the proposed Kalman filter have been implemented successfully in a PLC based industrial control system

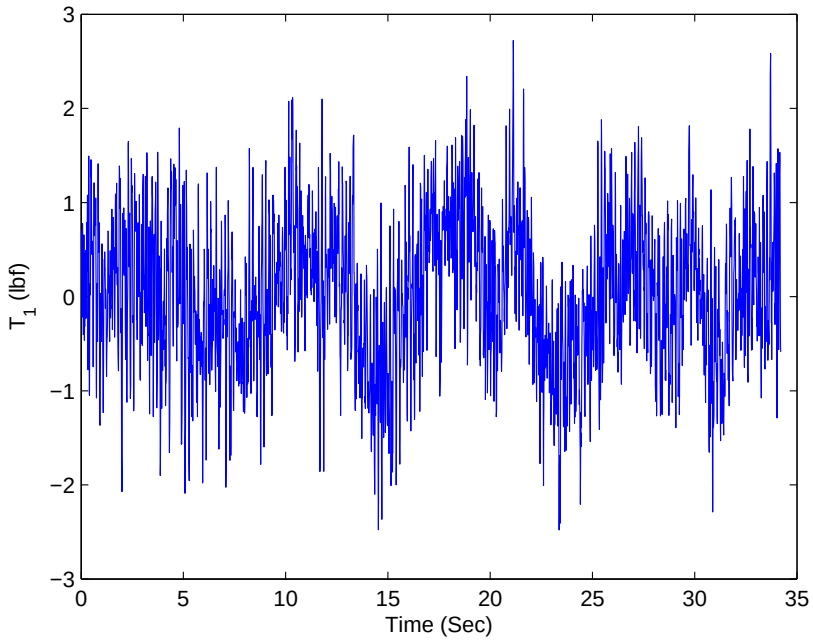

(a) T_1 Without Kalman Filter

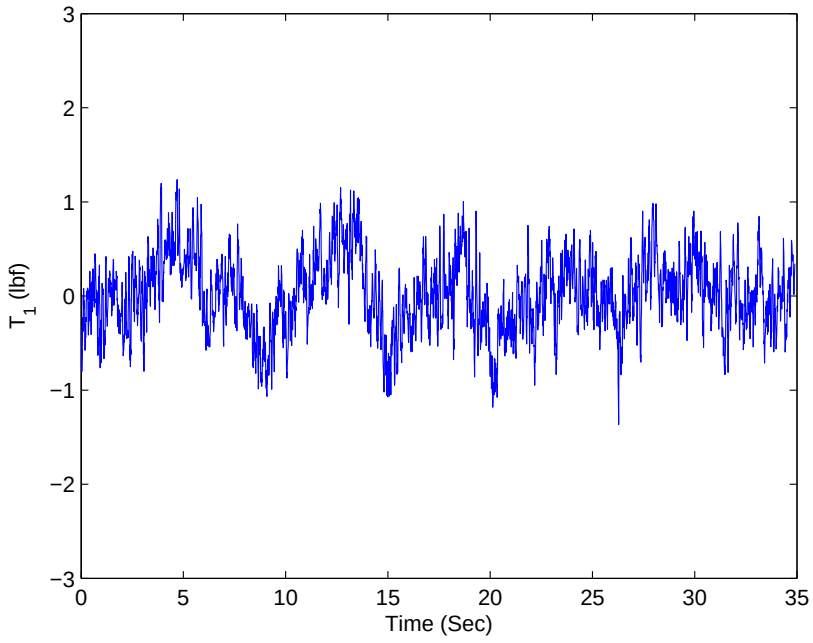

(b) T_1 With Kalman Filter

Figure 4.7: Tension Variation Comparison With Noise Amplitude $M = 5$ lbf

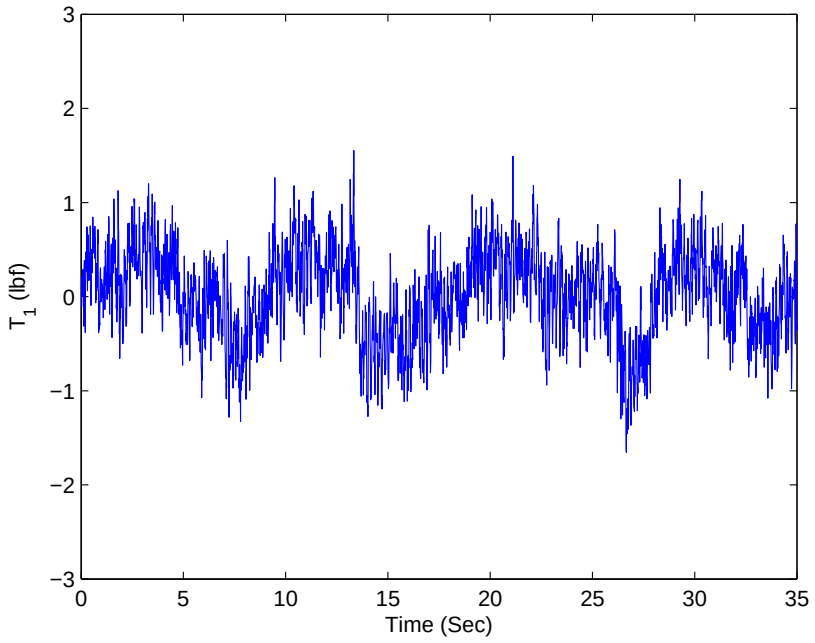

(a) T_1 Without Kalman Filter

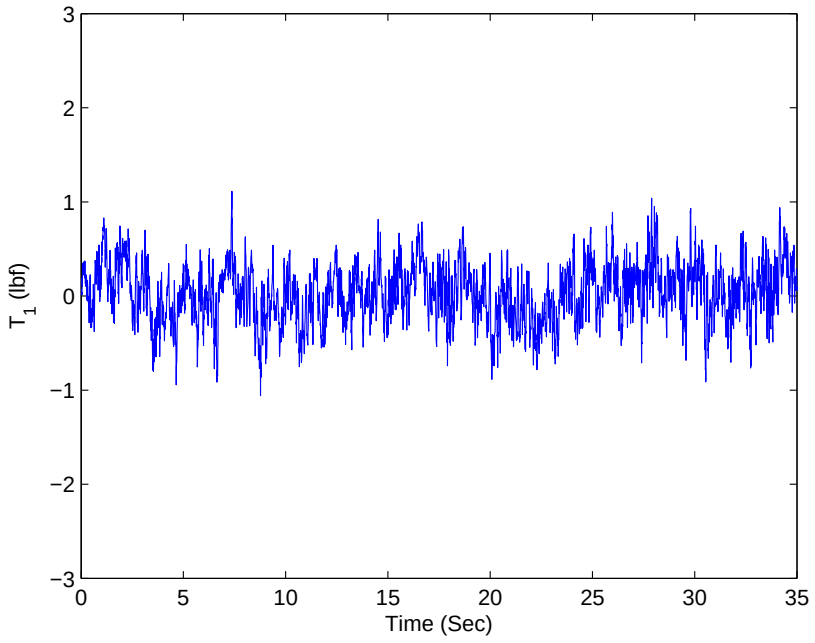

(b) T_1 With Kalman Filter

Figure 4.8: Tension Variation Comparison With Noise Amplitude $M = 2$ lbf

in EWL. The parameters of controllers and the Kalman filter are given and the experiment steps are listed in detail. The experimental data has been collected and analyzed. A performance index has been set based on the standard deviation of the tension feedback signal T_1 in order to evaluate the tension variation as well as the performance of the control system. The experimental results suggest that the proposed Kalman filter can improve tension control quality when heavy noise exists in the feedback loop.

Future work should focus on improving the tension dynamic model. In the current study, the tension error dynamics has been greatly simplified and been expressed as a transfer function $G_T(s)$. Concerns have been raised on whether this model can represent most of web tension's dynamic behavior. At the same time, the assumptions that the master speed roll runs exactly at reference velocity without any variations (that is $V_0 = 0$) and the previous web span tension t_0 is equal to reference tension t_r are not typically feasible in an industrial application. Thus, investigating these above issues in an effort to obtain a more comprehensive tension model and design a Kalman filter accordingly to improve tension control quality is reserved for the future.

CHAPTER 5

SUMMARY AND FURTHER WORK

5.1 Summary

Two groups have conducted research work on web handling process lines for years. The research and development engineers from industry have done a considerable amount of practical engineering work that has resulted in current understanding of web process line behavior. These engineers possess tremendous application experience and have the access to the practical web handling lines. Thus, they tend to use classic control system design methods to improve the performance of existing systems. They also place more emphasis on experimental results to solve practical problems than theoretical derivations. As the demands for higher productivity and better performance from the web processing industry increase, the classic design methods, such as transfer function based methods and PID control loops, may not fully meet the requirements. On the other hand, scholars in academia have proposed abundant system models and advanced modern control strategies for web handling process lines, but most of these research results still stay in the theoretical derivation or software simulation phase. Even in some cases that some experiments were designed to verify these new models and control strategies, the experimental platforms are relatively small and simple to simulate commercial web lines.

Thanks to the resources and support from Web Handling Research Center, a harmonious balance between theoretical studies and practical experiments is achieved in this thesis: a generalized system model is proposed in the state space form to predict resonant frequencies and a new tension signal filtering strategy is developed; all of

these are verified though experiments on a large-scale web line platform. Furthermore, experiments and data collection are completed using the standard commercial available devices including PLCs, AC drives and load cells.

An introduction to the mentioned real-time industrial control system and devices on a large web platform is given in Chapter 2, which serves as a basis for experimental verification.

In Chapter 3, web tension frequency response, especially the resonant frequencies of an idler system consisting of idle rollers and web spans between two driven rollers, is studied. A state space system model is proposed to predict these important resonant frequencies. The relationship between system parameters and the minimum resonant frequency is investigated as well. A close match between the experimental results from EWL and the model simulations verifies the proposed model to predict system resonant frequencies.

In Chapter 4, a discrete tension Kalman filter is designed based on the dynamic model in terms of state errors. The performance of the control system with proposed Kalman filter is compared with the original system. Substantial improvement in web tension error regulation is observed with the proposed filter in the case of a very noisy web tension signal.

5.2 Further Work

There are some challenging open topics to the problems studied in this thesis.

The Euclid Web Line itself is still needed to be improved and upgraded to meet the demanding requirements from research. A pivoted pendulum dancer is highly needed in order to conduct research on dancer system modeling and position control. The eccentricity (out of round) of the driven and idler rollers also introduces extra system tension disturbance, which needs to be investigated.

The frequency response and resonant frequencies of an idler system have been

studied in this thesis. Further research should be focused on a practical dancer system consisting of one dancer roller, several idlers and web spans between two driven rollers. During the modeling process of the idler system, the web tension dynamics is linearized without considering the transport of web strain from upstream to downstream spans, the slippage between web and roller, and friction. When modeling the dancer system, one should reconsider all of these factors and to find a system model that can predict the dynamic behavior of the system.

There has been much controversy and debate in the industry on the benefits and limitations of dancer feedback position control compared to load cell feedback tension control. Web handling equipment suppliers offer varying and often contradictory reasons for making this selection. Although comparison between these two systems can be found in [20, 7, 8, 9] through theoretical analyses and experiments, it is still worthwhile conducting further research based on the new idler system and dancer system models with an emphasis on the system's frequency response. Especially for the dancer system, the ideal model should not only include the dancer roller itself but also consider the effect of the other idler rollers upstream and downstream. Experiments should be done in a systematic way in order to compare the effects of these two systems in a practical large-scale web process line. Finally, guidelines based on solid theoretical research and experimental comparison should be proposed in order to facilitate the selection process.

The tension Kalman filter designed in this thesis can addresses the tension regulation problem due to the noises in the feedback path. Meanwhile, other advanced control methods should also be explored to improve web tension control quality and robustness in the entire web line in the presence of disturbances.

The tension control structure adapted in the EWL consists of two classical cascaded loops. This control strategy inherently requires that the inner loop (velocity loop) runs much faster than the outer loop (tension loop). This requirement limits

the tension loop dynamic behavior during transients, since the execution speed of the velocity loop is restricted by the drive processor's capacity and the motor's mechanical limitations. Further research could be conducted to investigate the possibility of bypassing the velocity loop, so that only one tension loop will be used in the tension control rollers.

BIBLIOGRAPHY

[1] G. Brandenburg, "New mathematical models for web tension and register error," in *Proceedings of the 3rd International IFAC Conference on Instrumentation and Automation in the Paper, Rubber and Plastics Industry*, vol. 1, 1977.

[2] D. P. D. Whitworth and M. C. Harrison, "Tension variations in pliable material in production machinery," *Applied Math. Modelling*, vol. 7, pp. 189–196, June 1983.

[3] J. J. Shelton, "Dynamics of web tension control with velocity or torque control.," in *Proceedings of the American Control Conference*, (Seattle, WA, USA), pp. 1423 – 1427, 1986.

[4] G. Young and K. Reid, "Lateral and longitudinal dynamic behavior and control of moving webs," *ASME Journal of Dynamic Systems, Measurement, and Control*, vol. 115, pp. 309–317, June 1993.

[5] P. R. Pagilla, N. B. Siraskar, and R. V. Dwivedula, "Decentralized control of web processing lines," *Control Systems Technology, IEEE Transactions on*, vol. 15, pp. 106–117, Jan. 2007.

[6] K.-H. Shin, *Distributed control of tension in multispan web transport systems.* Dissertation, Oklahoma State University, Oklahoma, United States, May 1991.

[7] J. J.Shelton, "Limitations to sensing of web tension by means of roller reaction forces," in *Proceedings of the Fifth International Conference on Web Handling* (J. Good, ed.), (Stillwater, Oklahoma, USA), June 1999.

[8] J. P.Ries, "Theoretical comparison of winding tension control methods," in *Proceedings of the Fifth International Conference on Web Handling* (J. Good, ed.), (Stillwater, Oklahoma, USA), June 1999.

[9] D.H.Carlson, "Considerations in the selection of a dancer or load cell based tension regulation strategy," in *Proceedings of the Sixth International Conference on Web Handling* (J. Good, ed.), (Stillwater, Oklahoma, USA), June 2001.

[10] B. Boulter, "Estimating modulus of elasticity, torque loss, and tension using an extended kalman filter," in *Proceedings of the Fifth International Conference on Web Handling* (J. Good, ed.), (Stillwater, Oklahoma, USA), June 1999.

[11] F. Mokhtari and P. Sicard, "State and parameter estimation in a winder based on second order polynomial approximations," *Industrial Electronics, 2006 IEEE International Symposium on*, vol. 1, pp. 378–383, July 2006.

[12] F. L. Lewis, *Applied optimal control & estimation : digital design & implementation*. Englewood Cliffs, N.J. : Prentice Hall, 1992.

[13] Rockwell Automation, Allen-Bradley, *AC Drives Using PWM Techniques*, January 2000. Publication DRIVES-WP002A-EN-P.

[14] Rockwell Automation, Allen-Bradley, *1336 FORCE Adjustable Frequency AC Drive User Manual*, January 1997. Publication 1336 FORCE-5.12.

[15] Rockwell Automation, Allen-Bradley, *ControlLogix Controllers User Manual*, May 2005. Publication 1756-UM001F-EN-P.

[16] Rockwell Automation, Allen-Bradley, *Logix5000 Controllers Common Procedures Programming Manual*, January 2005. Publication 1756-PM001H-EN-P.

[17] Rockwell Automation, Allen-Bradley, *ControlNet Modules in Logix5000 Control Systems*, November 2005. Publication CNET-UM001C-EN-P.

[18] Magnetic Power Systems, Inc., *Instruction Manual Model DTR - Digital Tension Readout*, March 1994. 850A96-1.

[19] Z. Liu, "Dynamic analysis of center-driven web winder controls," *Industry Applications Conference, 1999. Thirty-Fourth IAS Annual Meeting. Conference Record of the 1999 IEEE*, vol. 2, pp. 1388–1396 vol.2, 1999.

[20] N. Ebler, R. Arnason, G. Michaelis, and N. D'Sa, "Tension control: dancer rolls or load cells," *Industry Applications, IEEE Transactions on*, vol. 29, pp. 727–739, Jul/Aug 1993.

APPENDIX A

A Step-by-step Instructions on ControlNet Configuration

The step-by-step instructions on changing the configuration of the ControlNet communication bus used in EWL are summarized here to make the thesis self-contained. There are several ways available to set up ControlNet network, the method mentioned here has been employed for more than 2 years, and proved to be an effective way in the EWL control system environment. The following part gives detailed instructions on how to use RSLogix 5000 alone with RSNetWorx for ControlNet from Rockwell Automation to great a new or change the configuration of an existing ControlNet.

1. Add/Edit all the ControlNet hardware components in the RSLogix 5000 project file

    - For a new ControlNet Network, add all the local and remote ControlNet hardware components (including communication module, adapter and device) in the "I/O Configuration" part in the project file of the RSLogix 5000 according to the topology of the network shown in Figure A.1. When a new component is added, the component related parameters such as network address, RPI and communication format can be assigned.

    - For an existing ControlNet network, right click the components and select "Properties", then the module properties dialog box will appear as shown in Figure A.2. The component related ControlNet configuration such as network address and RPI can be modified in this dialog box. Notice,

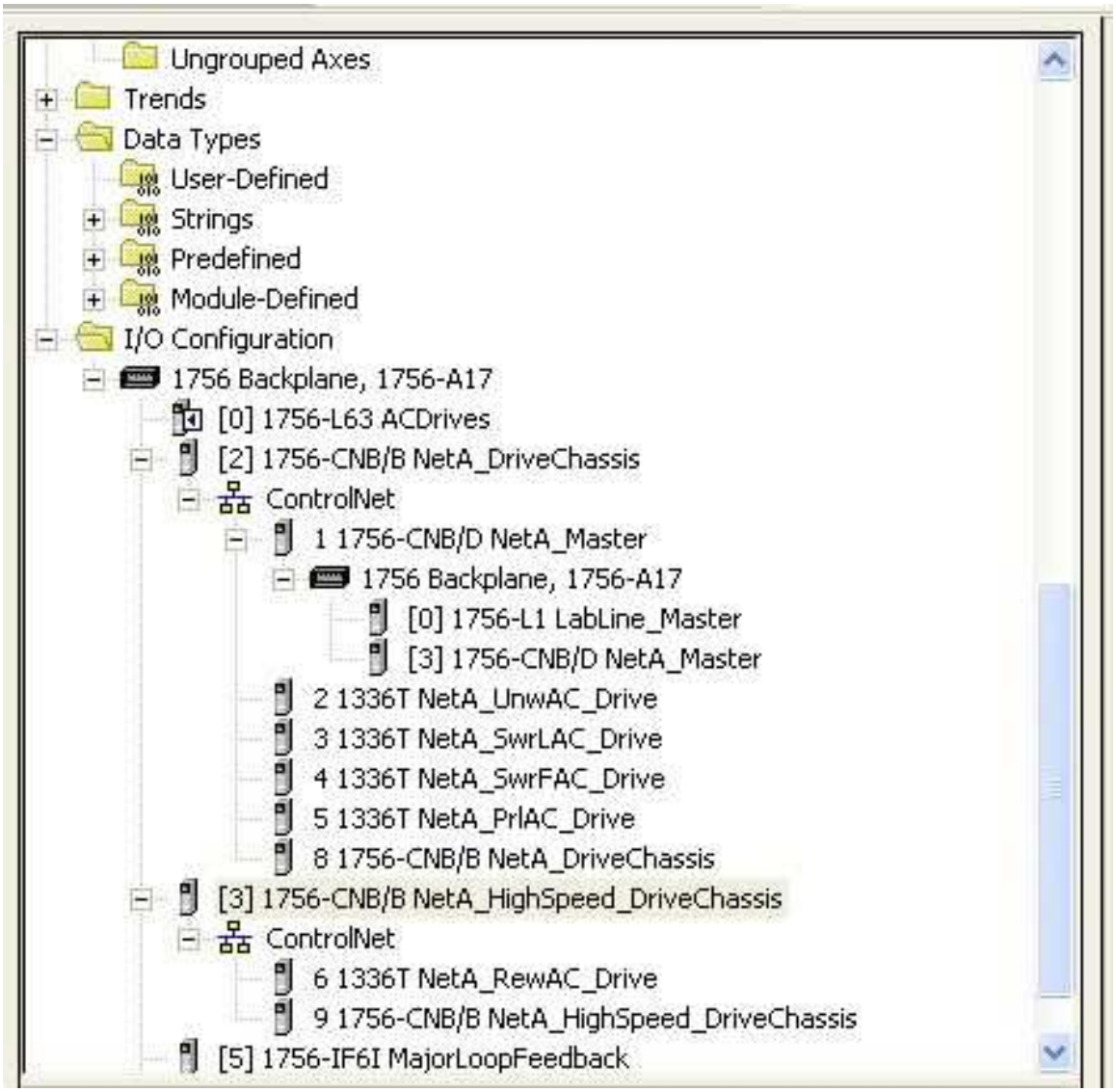

Figure A.1: ControlNet Hardware Configuration

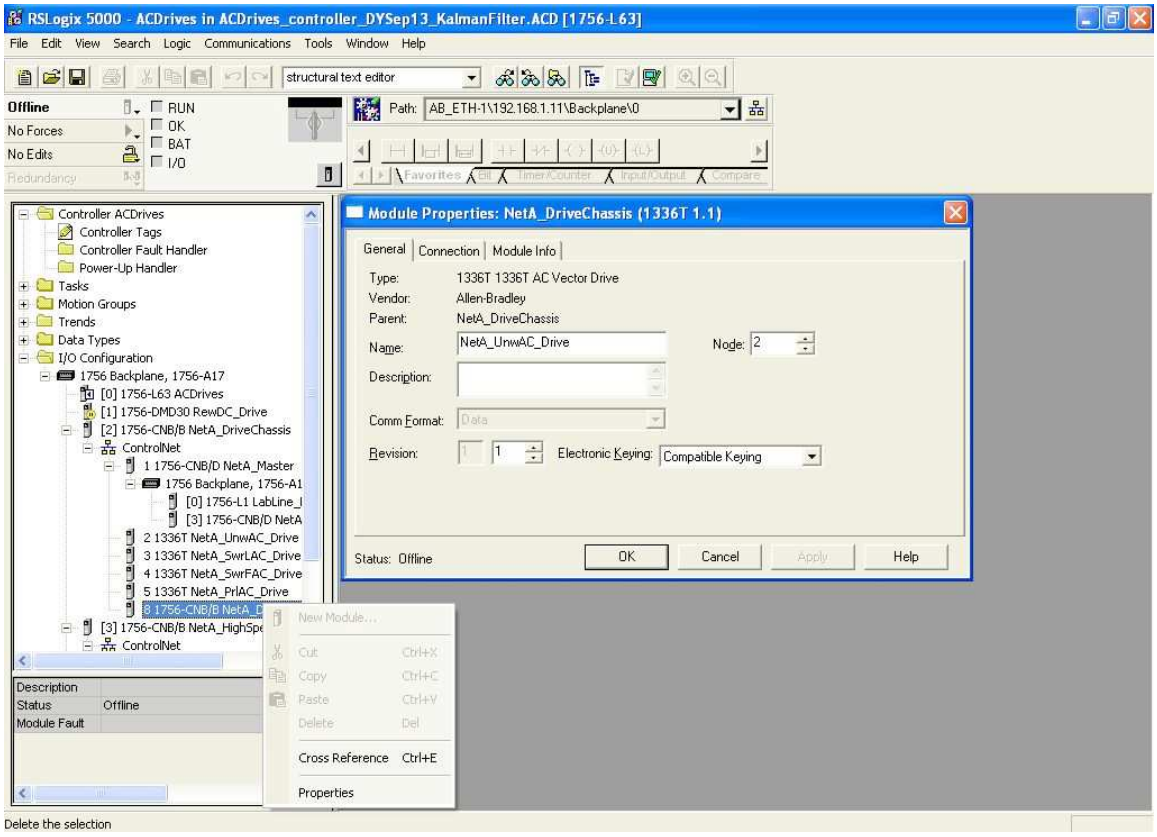

Figure A.2: ControlNet Module Properties Dialog Box

the communication format cannot be changed here, and the only way to change a component's communication format is to delete this module from the "I/O Configuration" tree and add it again with desired communication format.

2. *Download (NOT "Go Line")* the project file to the ControlLogix Controller.

   - When the project file is downloaded to the controller, the RSLogix 5000 also sends the ControlNet structure, configuration and parameters to the *local* communication module(s). In the case of Figure A.1, the *local* communication modules are located in slot 2 and 4.

3. Launch RSNetWorx for ControlNet and select "Network -¿ Online" or press

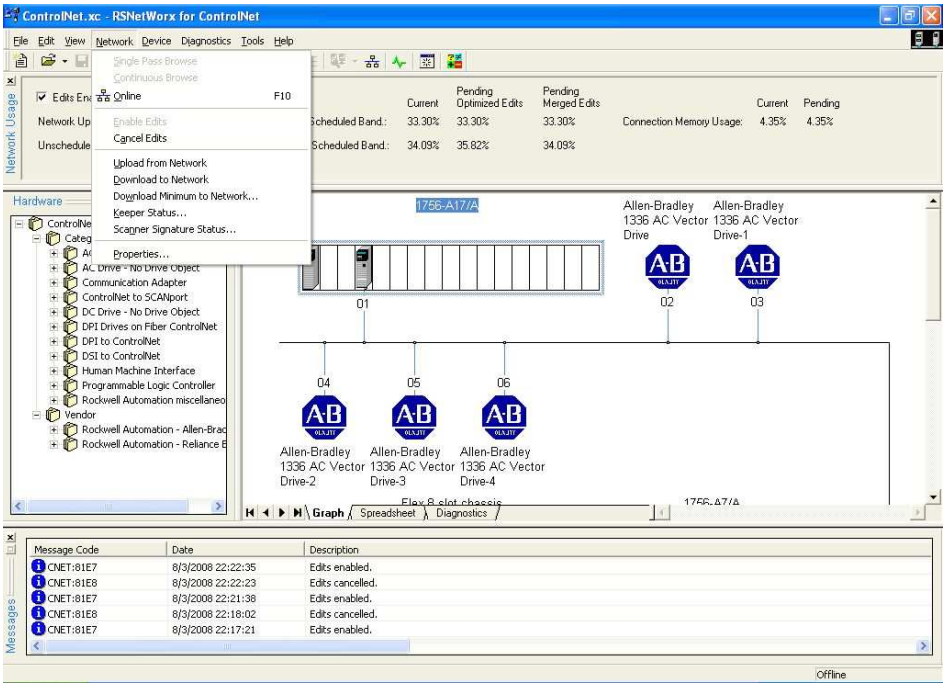

Figure A.3: Edit Mode of RSNetWorx for ControlNet

"F10" to go online.

4. Select "Network→Enable Edits", and the RSNetWorx for ControlNet will go into edit mode to allow the ControlNet configuration to be changed as shown in Figure A.3.

5. Select "Network→Properties...", then the ControlNet properties dialog box will appear, and the network related parameters such as NUT, network media configuration, SMAX can be set up here as shown in Figure A.4. This step can be bypassed if there is no need to change these network related parameters.

6. Select "File→Save", then the RSNetWorx for ControlNet will schedule the ControlNet and broadcast the new network configuration to all the nodes, meanwhile, the new configuration will be saved in all (local and remote) communi-

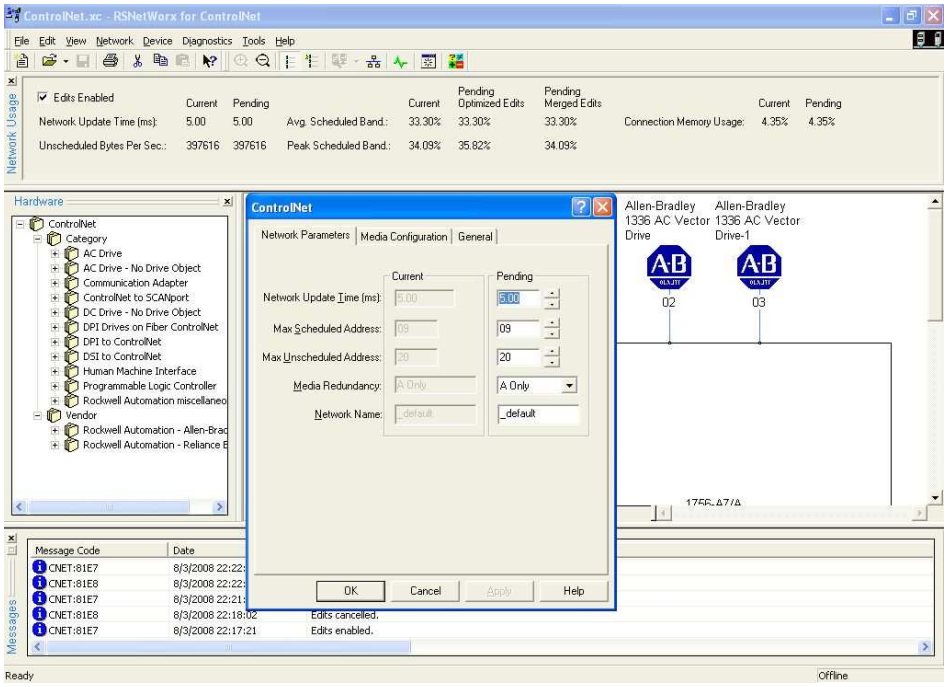

Figure A.4: ControlNet Network Properties Dialog Box

cation modules as well as controllers. Finally, the RSNetWorx for RSNetWorx will exist the edit mode.

7. Exit RSNetWorx for ControlNet. Open RSLogix 5000 with current project file, select "Communications→Go Online", and the project file will be automatically updated even no program code has been changed, since the ControlNet configuration has been renewed.

8. Save the updated project file in RSLogix 5000, and the ControlNet should work properly.

VITA

Yu Diao

Candidate for the Degree of

Master of Science

Thesis: RESONANT FREQUENCIES IN WEB LINES AND FILTERING OF WEB TENSION

Major Field: Mechanical Engineering

Biographical:

Personal Data: Born in Chengdu, Sichuan, P.R.China on June 27, 1981, the son of Xuefeng Diao and Youjun Ge.

Education: Received the B.E. degree from Shanghai Jiao Tong University, Shanghai, P.R.China in 2003, in Automation Science and Electrical Engineering; Completed the requirements for Master of Science degree with a major in Mechanical Engineering at Oklahoma State University in December, 2008.

Experience: Research Assistant at Oklahoma State University from January 2006 to present; Teaching Assistant at Oklahoma State University from August 2005 to August 2006; Product Engineer at Schneider Electric Co., Ltd. Shanghai, China from July 2003 to August 2005.

Name: Yu Diao Date of Degree: December, 2008

Institution: Oklahoma State University Location: Stillwater, Oklahoma

Title of Study: RESONANT FREQUENCIES IN WEB LINES AND FILTERING OF WEB TENSION

Pages in Study: 95 Candidate for the Degree of Master of Science

Major Field: Mechanical Engineering

Scope and Method of Study: The thesis proposes a dynamic model for an idler system and investigates the relationship between the idler system's minimum resonant frequency and the system parameters. A Kalman filter is designed and implemented in the web tension feedback loop to improve the tension control performance. A large experimental platform, which mimics most of the features of an industrial web process line, is used to verify the proposed idler system model experimentally and to demonstrate the effects of the tension Kalman filter.

Findings and Conclusions: A state space system model is proposed to predict the resonant frequencies of an idler system consisting of idler rollers and web spans between two driven rollers. A close match between the experimental results and the model simulations validate the correctness of the dynamic model. The relationship between system parameters and the system's minimum resonant frequency is investigated through analytical and numerical analyses. An analytical approximation of the minimum resonant frequency is developed for a special class of idler systems consisting of equal span lengths and any number of idle rollers. A Kalman filter is designed based on the web span tension dynamic model in terms of state errors. Extensive comparative experiments with and without the Kalman filter show improvement in the web tension signal when the Kalman filter is used.

ADVISOR'S APPROVAL: _____